Journal of *Marine Science and Engineering*

MDPI

Article

Event-Triggered Neural Adaptive Distributed Cooperative Control for the Multi-Tug Towing of Unactuated Offshore Platform with Uncertainties and Unknown Disturbances

Shaolong Geng [1], Yulong Tuo [1,2,*], Yuanhui Wang [3], Zhouhua Peng [1,2] and Shasha Wang [1,2]

[1] College of Marine Electrical Engineering, Dalian Maritime University, Dalian 116026, China; gengshaolong1127@163.com (S.G.); zhpeng@dlmu.edu.cn (Z.P.); wangshashadmu@dlmu.edu.cn (S.W.)
[2] Dalian Key Laboratory of Swarm Control and Electrical Technology for Intelligent Ships, Dalian 116026, China
[3] College of Intelligent System Science and Engineering, Harbin Engineering University, Harbin 150001, China; wangyuanhui@hrbeu.edu.cn
* Correspondence: tuoyulong@dlmu.edu.cn

Abstract: An event-triggered neural adaptive cooperative control is proposed for the towing system (TS) with model parameter uncertainties and unknown disturbances. Different from ordinary multi-vessel formation control, the tugs and unactuated offshore platform in the TS are connected together by towlines, and the resultant tension of the towlines serves as the actual drag force for the platform. Initially, based on the radial basis function neural network (RBFNN), an adaptive RBFNN is designed to compensate unknown disturbances and model parameter uncertainties of the TS, and we use minimal learning parameter (MLP) algorithm to reduce the online learning parameters of adaptive RBFNN. Combined with dynamic surface technology and event-triggered control (ETC) mechanism, an event-triggered neural adaptive virtual controller is designed to obtain the desired drag force of the platform. According to the quadratic programming algorithm, the desired drag force is allocated as the desired tensions of towlines. Subsequently, the desired towline length and the desired position information of the tugs are obtained sequentially through the towline model and the position relationship between the tugs and the platform. Then, according to the desired positions of tugs, an event-triggered neural adaptive distributed cooperative controller is designed for achieving the multi-tug towing of the offshore platform. The ETC mechanism is introduced to reduce the communication burden within the TS and the execution frequency of the tugs' thrusters. Finally, the stability of the closed-loop system is proven using the Lyapunov theory, and the ETC mechanism proves that no Zeno behavior occurs. The effectiveness of the ETC mechanism and the MLP-based adaptive RBFNN on the controllers of TS is verified through simulations and comparison analysis.

Keywords: towing system; event triggered; neural network; minimum learning parameter algorithm

Citation: Geng, S.; Tuo, Y.; Wang, Y.; Peng, Z.; Wang, S. Event-Triggered Neural Adaptive Distributed Cooperative Control for the Multi-Tug Towing of Unactuated Offshore Platform with Uncertainties and Unknown Disturbances. *J. Mar. Sci. Eng.* **2024**, *12*, 1242. https://doi.org/10.3390/jmse12081242

Academic Editors: Xu Fang, Chao Deng, Shankar A. Deka, Jitao Li and Heling Yuan

Received: 30 May 2024
Revised: 19 July 2024
Accepted: 22 July 2024
Published: 23 July 2024

1. Introduction

Multi-tug towing is a common water transportation method for unactuated offshore platforms. Different from ordinary multi-vessel formation control, the tugs and platform in the towing system (TS) are connected together by towlines, and the combined tension of the towlines serves as the actual drag force for the platform. Compared to the umbilical cable [1] of underwater vehicles, the damping coefficient of the towlines in the TS is relatively large, and even a slight change in length can significantly impact the combined tension. This poses strict requirements for the precision of the TS cooperative control. In actual water operations, unknown disturbances and model uncertain parameters are the main reasons affecting control effect for the marine vehicles, such as the autonomous

underwater vehicle [2], unmanned surface vessel [3], and TS [4]. Additionally, the proposed cooperative control schemes [5–9] did not account for unknown disturbances, resulting in poor applicability. Ref. [10] proposed a parameter adaptive method to handle the environmental disturbances of the TS, but the model parameters of the system were assumed to be known. Therefore, how to deal with the unknown disturbances and uncertainties on multi-tug cooperative control is still a key issue that urgently needs to be addressed.

Due to the strong approximation and learning ability, the radial basis function neural network (RBFNN) has been widely applied to deal with the uncertainties [11–13]. Although there are few studies on RBFNN for the TS, we can still learn from the applications of RBFNN in multi-agent control systems and vessels control systems. Ref. [14] proposed a local RBFNN distributed cooperative learning control strategy for multi-agent collaborative systems with uncertain dynamics. Ref. [15] used the Chebyshev neural network to approximate the bounded external disturbances of spacecraft. Ref. [16] proposed an adaptive neural network based on a backstepping strategy, which can effectively mitigate the impact of disturbances on vessels. Ref. [17] employed an RBFNN to mitigate the effects of unknown nonlinearities on vessels with unidentified dead zones in their rudder angles. However, there are a large number of learning parameters that need to be adjusted online in these schemes, which will lead to an increase in the computational complexity of the TS. The amount of computation will limit the application of the adaptive RBFNN in the TS.

In addition, the TS requires low-velocity navigation during transportation, which results in long towing task completion time. On one hand, long time navigation will result in the long-term high-frequency action of tugs' thrusters, reducing the service life of thrusters. On the other hand, the tugs need to communicate continuously with the platform and adjacent tugs during the navigation, but traditional continuous trigger control (CTC) will lead to wasted resources and energy [18]. To the best of our knowledge, there is no relevant research that has addressed the high-frequency response and communication resource waste of the TS. Fortunately, event-triggered control (ETC) has gained attention for its advantages in reducing transmission and computational burdens [19–22].

At present, ETC is widely applied in control systems. Ref. [19] introduced a drone control system with an event-driven mechanism that responds to specific triggers, effectively reducing communication frequency and enhancing the system's flexibility. Ref. [20] discussed the time-varying formation problem of high-order multi-agent system under external disturbances and proposed an event-triggered integral sliding mode control strategy, which saves energy consumption and avoids triggering Zeno behavior in time series. Ref. [21] designed an interleaved periodic ETC for cooperative unmanned surface vessels to prevent communication delays and actuator faults. Ref. [22] designed an asynchronous event-triggered scheme for nonlinear entities, conserving the network resources of networked control systems. Obviously, we can introduce ETC mechanism in the distributed collaborative control scheme of TS, which can reduce the communication burden and the action frequency for tugs' thrusters.

Based on the above discussion, we propose an event-triggered neural adaptive cooperative control for the TS with model parameter uncertainties and unknown disturbances. Firstly, an adaptive RBFNN is designed to compensate for disturbances and model parameter uncertainties of the TS based on the minimal learning parameter (MLP) and RBFNN. Based on the adaptive RBFNN, an event-triggered neural adaptive virtual controller of the platform is designed to obtain the desired drag force of the platform. Subsequently, according to the quadratic programming (QP) algorithm, the desired drag force is allocated as the desired tensions of towlines, and the desired towline length and the desired position information of the tugs are obtained sequentially through the towline model and the position relationship between the tugs and the platform. Then, according to the desired positions of tugs, we design an event-triggered neural adaptive distributed cooperative controller, where the ETC mechanism is introduced to reduce the

communication burden and the action frequency for tugs' thrusters, and the prominent highlights of this paper are organized as follows:

- Different from the simplified model of TS in [5–10], the parameter uncertainty and unknown disturbances are considered in our paper to establish a more realistic mathematical model for TS. Then, an MLP-based adaptive RBFNN is designed to compensate uncertainty and disturbances. Compared to the RBFNNs in [12–15], only three online learning parameters need to be considered for our MLP-based adaptive RBFNN, thus reducing the design and computational burden caused by the large number of learning parameters.
- Unlike the collaborative control methods of the TS [4–10], we design an event-triggered neural adaptive cooperative controller to reduce the communication burden and the frequency of actions for the tugs' thrusters. Moreover, the ETC mechanism does not significantly affect the control performance of the TS.

The principal contents of this paper include the following: Section 2 introduces the RBFNN, the mathematical model of the TS, and the control objectives; Section 3 proposes an event-triggered neural adaptive cooperative control for the TS and stability analysis; Section 4 validates the effectiveness of the proposed MLP-based adaptive RBFNN and ETC mechanism; and Section 5 provides a summary of the entire paper.

Lastly, to enhance the overall readability of this paper, a dedicated nomenclature section has been added for the abbreviations and symbols as below.

2. Preliminaries and Problem Formulation

2.1. Radial Basis Function Neural Network

Lemma 1. *Based on [23], for a continuous nonlinear function* $V(\delta): R^n \to R^k$ *and any positive constant* μ*, the RBFNN can approximate* $V(\delta)$ *as follows:*

$$V(\delta) = W^T h(\delta) + \mu \tag{1}$$

where $\forall \delta \in \Omega_\delta \subset R^n$, $W \in R^{m \times k}$ *is the optimal weight matrix;* m *represents the number of hidden layer neurons;* $h(\delta) = [h_1(\delta) \cdots h_m(\delta)] \in R^{m \times 1}$ *represents the neuron basis function, where* $\|h(\delta)\| \le \bar{h}$ *and* $\bar{h}$ *is a positive constant; and* $\mu \in R^k$ *represents the approximation error, where* $\|\mu\| \le \bar{\mu}$.

2.2. Towline Model

We use the catenary model to represent the towlines connecting the tugs and the platform [24,25]. In Figure 1, we denote the tension in the towline as T_R, T_H is the effective force applied to the platform and tugs, and D_H and L_R represent the horizontal and actual length of the towlines. G_R denotes the gravitational force acting on the towlines. The catenary model is as follows:

$$T_H = \left(D_H - \frac{2T_H}{\sigma} \sinh^{-1}\left(\frac{\sigma L_R}{2T_H} \right) \right) \frac{EA}{L_R} \tag{2}$$

where T_H refers to the horizontal tension of the towlines, σ is the density of towlines, and E and A are the towlines' elastic modulus and cross-sectional area.

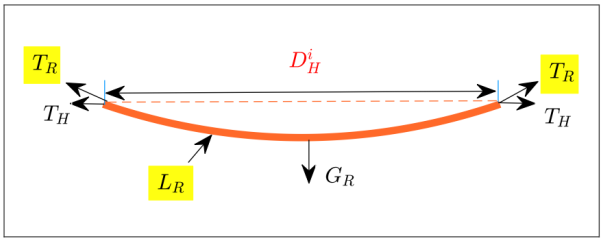

Figure 1. Towline model.

2.3. Dynamic Models of Tugs and the Offshore Platform

In this paper, the connection relationship between the platform and tugs of the TS are shown in Figure 2.

The mathematical model of $i-th$ $(i=1,\ldots,4)$ tug is described by [26]:

$$\begin{aligned} \dot{\eta}_i &= J(\psi_i)v_i, \\ M_i\dot{v}_i + D_i v_i + g_i &= \tau_i + \tau_h^i + \tau_w^i \end{aligned} \tag{3}$$

where $\eta_i = [x_i, y_i, \psi_i]^T$ represents the north and east positions of the tug in the earth-fixed coordinate system, $v_i = [u_i, v_i, r_i]^T$ represents the velocity in the body-fixed coordinate system, $J(\psi_i)$ is the transformation matrices, and M_i and D_i are inertial matrices and damping matrices, respectively. τ_w^i and g_i refer to disturbance forces and unmodeled dynamics. $\tau_h^i = B_i T_H^i$ denotes the effort vector induced by the horizontal tension, where $B_i = [\cos(\phi_i), \sin(\phi_i), 0]^T$ and the definitions of ϕ_i are described in Figure 2.

Due to the similarity between the platform and tug models, the platform model is shown below:

$$\begin{aligned} \dot{\eta}_0 &= J(\psi_0)v_0 \\ M_0\dot{v}_0 + D_0 v_0 + g_0 &= \tau_0 + \tau_w^0 \end{aligned} \tag{4}$$

where $\tau_0 = B_0 T$ represents the drag force exerted by the tugs though towlines, and $T = \left[T_H^1,\ T_H^2,\ T_H^3,\ T_H^4\right]^T$ and B_0 are given below:

$$B_0 = \begin{bmatrix} \cos(\theta_1) & \cos(\theta_2) & \cos(\theta_3) & \cos(\theta_4) \\ \sin(\theta_1) & \sin(\theta_2) & \sin(\theta_3) & \sin(\theta_4) \\ l_{x1}\sin(\theta_1) - l_{y1}\cos(\theta_1) & l_{x2}\sin(\theta_2) - l_{y2}\cos(\theta_2) & l_{x3}\sin(\theta_3) - l_{y3}\cos(\theta_3) & l_{x4}\sin(\theta_4) - l_{y4}\cos(\theta_4) \end{bmatrix} \tag{5}$$

where θ_i refers to the angle between the towlines and the platform's heading in the earth-fixed coordinate system, (l_{xi}, l_{yi}) specifies the location of the tow point on the platform, and other definitions are consistent with the tug model (3).

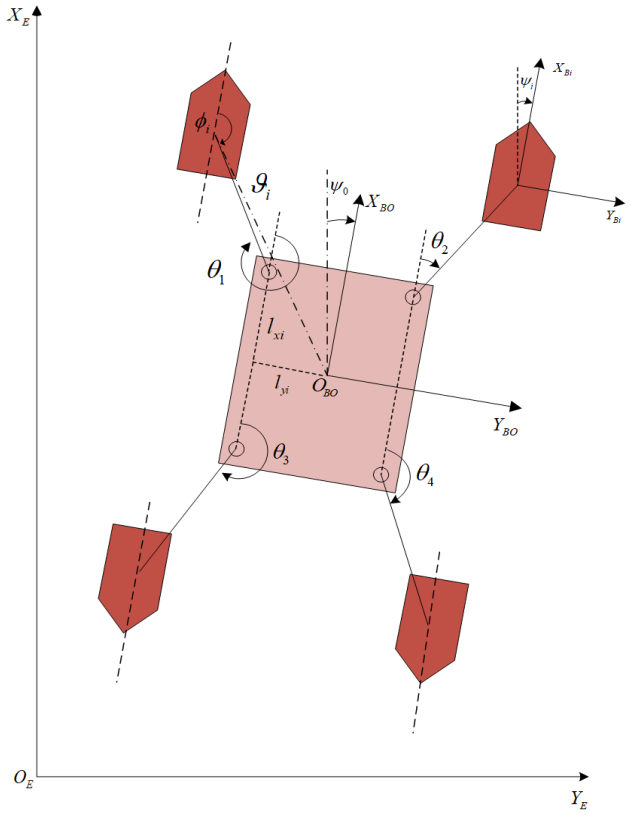

Figure 2. The connection relationship of the TS.

2.4. The Time-Variant Relative Position

To obtain the desired position information of the tugs, we introduce the time-variant relative position $\eta_i^{t-v} = \left[\eta_{xi}^{t-v} \quad \eta_{yi}^{t-v} \quad \eta_{zi}^{t-v}\right] \in R^3$ [10]:

$$\eta_i^{t-v} = q_i + p_i^d \tag{6}$$

where $q_i = \eta_i^{tow} - \eta_0$, η_i^{tow} is the attachment point of each towlines on the platform, $q_i(3) = 0$; $p_i^d = d_i^H B_i^d$, d_i^H refers to the towlines' desired horizontal length; $B_i^d = [\cos(\theta_i + \psi_0), \sin(\theta_i + \psi_0), \rho_i / d_i^H]^T$ with constant ρ_i.

Assumption 1. *The parameters M_0, M_i, D_0, and D_i $(i = 1, \ldots, 4)$ of the TS model are unknown.*

Assumption 2. *The desired trajectory η_d of the platform and the desired trajectory $\eta_0 + \eta_i^{t-v}$ of the $i-th$ tug are continuous and bounded.*

Assumption 3. *The unmodeled dynamics and disturbance g_0, g_i, τ_w^0, and τ_w^0 are continuous and bounded.*

2.5. Control Objective

The objective is to design an event-triggered neural adaptive distributed cooperative controller for the TS under unknown disturbances and uncertain parameters, with the following aims:

P1. The designed adaptive RBFNN with MLP can compensate the uncertain parameters and unknow disturbances of the TS.

P2. The platform can be towed by the tugs to follow the reference trajectory η_d, and tugs can follow η_d^i, where $\eta_d^i = \eta_0 + \eta_i^{t-v}$.

P3. The designed ETC mechanism can effectively reduce the communication frequency of the TS and the action frequency of the tugs' thrusters.

3. Main Results

To enhance the clarity and comprehensibility of our detailed implementation, the schematic for the event-triggered neural adaptive distributed cooperative control scheme of the TS is given in Figure 3. An event-triggered neural adaptive cooperative control is proposed for multi-tug coordinated towing of unactuated offshore platform under the disturbances and uncertainties in this section. Initially, we proposed an event-triggered neural adaptive virtual controller to acquire desired drag force for the offshore platform. Subsequently, the desired drag force is allocated to the desired tensions by the proposed allocation scheme. Then, we designed an event-triggered neural adaptive distributed cooperative controller to achieve the multi-tug towing of offshore platform. Finally, the stability of the closed-loop system is proven using the Lyapunov theory, and the ETC mechanism proves that no Zeno behavior occurs.

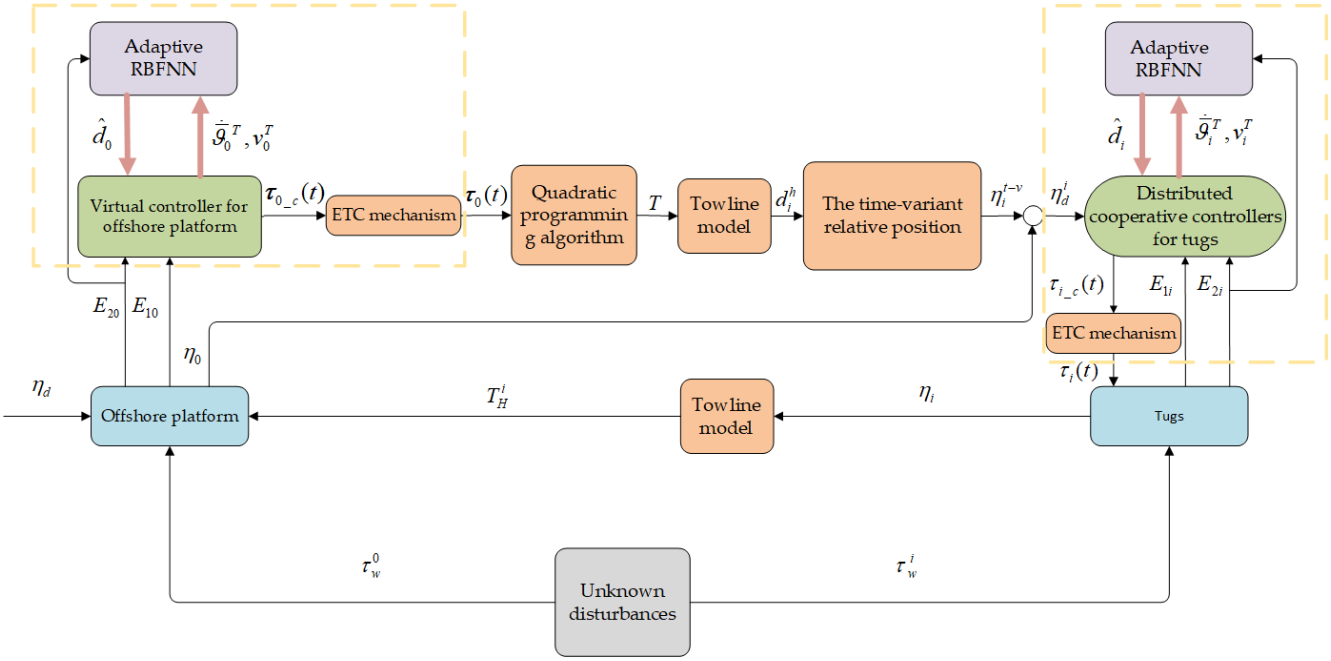

Figure 3. The schematic for the event-triggered neural adaptive distributed cooperative control scheme of the TS.

3.1. Event-Triggered Neural Adaptive Virtual Controller for Offshore Platform

In this subsection, an event-triggered neural adaptive virtual controller is proposed for the offshore platform. Firstly, the two error of the platform is defined as follows:

$$\begin{cases} \boldsymbol{E}_{10} = \boldsymbol{\eta}_0 - \boldsymbol{\eta}_d \\ \boldsymbol{E}_{20} = \boldsymbol{v}_0 - \boldsymbol{\vartheta}_0 \end{cases} \tag{7}$$

where $E_{20} = \begin{bmatrix} E_{20,1} & E_{20,2} & E_{20,3} \end{bmatrix}^T$, the control law $\vartheta_0 \in R^3$ for the platform can be obtained as follows:

$$\boldsymbol{\vartheta}_0 = \boldsymbol{J}(\boldsymbol{\psi})_0^T(-\boldsymbol{K}_{10}\boldsymbol{E}_{10} + \dot{\boldsymbol{\eta}}_d). \tag{8}$$

To simplify the computation of the derivative of ϑ_0, a first-order filter is introduced to obtain $\bar{\vartheta}_0$ as follows:

$$\boldsymbol{k}\dot{\bar{\vartheta}}_0 = \vartheta_0 - \bar{\vartheta}_0, \quad \bar{\vartheta}_0(0) = \vartheta_0(0) \tag{9}$$

where $\boldsymbol{k} > 0$ is a predetermined time constant.

Based on the (9), (4), we can obtain the derivative of (7) as follows:

$$\begin{cases} \dot{\boldsymbol{E}}_{10} = \boldsymbol{J}(\boldsymbol{\psi})_0 \boldsymbol{v}_0 - \dot{\boldsymbol{\eta}}_d \\ M_0 \dot{\boldsymbol{E}}_{20} = \boldsymbol{\tau}_0 + \boldsymbol{d}_0 \end{cases} \tag{10}$$

where $\boldsymbol{d}_0 = \boldsymbol{\tau}_w^0 - \boldsymbol{D}_0 \boldsymbol{v}_0 - \boldsymbol{g}_0 - \boldsymbol{M}_0 \dot{\bar{\vartheta}}_0$ represents the total disturbances and uncertainties of the platform. Since $\boldsymbol{d}_0$ is unknown in the actual towing system, this scheme employs the RBFNN to estimate $\boldsymbol{d}_0$ as follows:

$$\hat{\boldsymbol{d}}_0 = \boldsymbol{W}_0^T \boldsymbol{h}_0(\boldsymbol{\delta}_0) + \boldsymbol{\mu}_0 \tag{11}$$

where $\hat{\boldsymbol{d}}_0$ is the estimation of $\boldsymbol{d}_0$, $\boldsymbol{W}_0 = \begin{bmatrix} W_1^T & 0_{1\times m} & 0_{1\times m} \\ 0_{1\times m} & W_2^T & 0_{1\times m} \\ 0_{1\times m} & 0_{1\times m} & W_3^T \end{bmatrix}$ is the optimal weight matrix, $W_n \in R^{m\times 1}(n = 1,2,3)$, m represents the number of neurons, $\boldsymbol{h}_0(\boldsymbol{\delta}_0) = \left[h_{0,1}^T(\delta_{0,1}) \quad h_{0,2}^T(\delta_{0,2}) \quad h_{0,3}^T(\delta_{0,3}) \right]^T$, with $h_n(\delta_n) \in R^{m\times 1}$, $\boldsymbol{\delta}_0 = \left[1 \quad \dot{\bar{\vartheta}}_0^T \quad v_0^T \right]^T$, and $\boldsymbol{\mu}_0 = \left[\mu_{0,1} \quad \mu_{0,2} \quad \mu_{0,3} \right]$.

According to Lemma 1, the norm of d_0 satisfies the following inequality:

$$\left\| d_{0,n} \right\| = \left\| W_{0,n}^T h_{0,n}(\delta) + \mu_{0,n} \right\| \le \chi_{0,n} \xi_{0,n} \tag{12}$$

where $\chi_{0,n} = \max\left\{ \left\| W_{0,n} \right\|, \bar{\mu}_{0,n} \right\}$, $\xi_{0,n} = 1 + \left\| h_{0,n}(\delta_{0,n}) \right\|$.

Based on the MLP algorithm, the control effort $\tau_{0\_c}(t)$ is designed as follows:

$$\boldsymbol{\tau}_{0\_c}(t) = -\boldsymbol{K}_{20} E_{20} - \hat{\boldsymbol{d}}_0 \tag{13}$$

where $\hat{\boldsymbol{d}}_0 = \hat{\boldsymbol{\rho}}_0 \boldsymbol{\varepsilon}_0 E_{20}$, $\boldsymbol{\tau}_{0\_c}(t) = \left[\tau_{0\_c,1}(t) \quad \tau_{0\_c,2}(t) \quad \tau_{0\_c,3}(t) \right]$, $\boldsymbol{\rho}_0 = diag(\rho_{0,1}, \rho_{0,2}, \rho_{0,3})$, $\hat{\boldsymbol{\rho}}_0 = diag(\hat{\rho}_{0,1}, \hat{\rho}_{0,2}, \hat{\rho}_{0,3})$ is the estimation of $\boldsymbol{\rho}$, $\rho_{0,n} = \chi_{0n}^2 (n = 1,2,3)$, $\boldsymbol{\varepsilon}_0 = diag(\varepsilon_{0,1}, \varepsilon_{0,2}, \varepsilon_{0,3})$, with $\varepsilon_{0,n} = \xi_{0,n}^2 / (4\delta_{0,n}^2)$, and $\delta_{0,n}$ represents the positive constant. The update rate of $\hat{\rho}_0$ as follows:

$$\dot{\hat{\rho}}_{0,n} = \beta_{0,n} \left\{ \varepsilon_{0,n} E^2{}_{20,n} - \gamma_{0,n} \left[\hat{\rho}_{0,n} - \hat{\rho}_{0,n}(0) \right] \right\} \tag{14}$$

According to ETC, the final control law is designed as follows:

$$\tau_{0,n}(t) = \tau_{0\_c,n}(t_{0,n}^s), \ \forall t \in [t_{0,n}^s, t_{0,n}^{s+1}), \ \text{n=1,2,3} \tag{15}$$

where $\boldsymbol{\tau}_0(t) = \left[\tau_{0,1}(t) \quad \tau_{0,2}(t) \quad \tau_{0,3}(t) \right]$, and $t_{0,n}^s$ is the triggering time instant of the s-th event. The triggering conditions are as follows:

$$\begin{cases} t_{0,n}^s = \inf\left\{ t \in R \,|\, \left| E_{0,n} \right| \ge \alpha_{0,n} \right\} \\ E_{0,n} = \boldsymbol{\tau}_{0\_c,n}(t_{0,n}^{s-1}) - \boldsymbol{\tau}_{0,n}(t_{0,n}^s) \end{cases} \tag{16}$$

where $\alpha_{0,n} \in R$, which satisfies $0 < \alpha_{0,n} < \bar{\alpha}_{0,n}$, with constants $\bar{\alpha}_{0,n}$. If the triggering condition of (16) is not met, $\tau_{0,n}(t)$ remains constant $\tau_{0\_c,n}(t_{0,n}^{s-1})$. When triggering condition (16) is met, the current triggering time instant is marked as $t_{0,n}^s$, and control input $\tau_{0,n}(t)$ will change to $\tau_{0\_c,n}(t_{0,n}^s)$.

Remark 1. *For the input signal triggering mechanism, the threshold triggering conditions [27] and the dynamic triggering conditions [28] may exhibit Zeno behavior. The fixed threshold triggering condition for the control signal can effectively prevent Zeno behavior. Therefore, this paper adopts fixed threshold triggering conditions.*

Based on (10), (13), and (14) and defining $\tilde{\rho}_{0,n} = \hat{\rho}_{0,n} - \rho_{0,n}$, we obtain the following:

$$\begin{cases} \dot{\boldsymbol{E}}_{10} = -K_{10}\boldsymbol{E}_{10} + \boldsymbol{J}(\boldsymbol{\psi})_0\left(\boldsymbol{E}_{20} + \boldsymbol{q}_0\right) \\ M_0\dot{\boldsymbol{E}}_{20} = -\boldsymbol{K}_{20}\boldsymbol{E}_{20} - \hat{\boldsymbol{\rho}}_0\boldsymbol{\varepsilon}_0\boldsymbol{E}_{20} + \boldsymbol{d}_0 \\ \dot{\tilde{\rho}}_{0,n} = \beta_{0,n}\left\{\varepsilon_{0,n}E^2{}_{20,n} - \gamma_{0,n}\left[\hat{\rho}_{0,n} - \hat{\rho}_{0,n}(0)\right]\right\} \end{cases} \tag{17}$$

where $\boldsymbol{q}_0 = \overline{\boldsymbol{\vartheta}}_0 - \boldsymbol{\vartheta}_0$.

3.2. Control Allocation of the Drag Force

The actual drag force of the offshore platform is provided through towlines linked with tugs [10,25]. The optimal desired tension of each towline is computed by the quadratic programming (QP) algorithm [29]. The objective function is constructed as below:

$$\min J = T^T\Omega T + s^T Q s \tag{18}$$

subject to

$$\begin{cases} s = \tau_0(t) - B_0 T \\ T_h^{\min} \le T_h^i \le T_h^{\max} \end{cases} \quad i = 1,2,3,4 \tag{19}$$

where $T_h^{\min}$ and $T_h^{\max}$ represent the minimum and maximum horizontal tensions of towlines, and Ω and Q are weighting matrices.

Then, combined with the T_h^i and the towline model (2), the desired horizontal distance d_i^H and the actual horizontal tension T_H^i can be gained. The time-variant relative position υ_i can be obtained by (6).

Remark 2. *There are some typical algorithms to solve the optimal desired tension problem [25,29–31]. Linear programming (LP) is not suitable for quadratic objective function problems [30]. Nonlinear programming (NLP) [31] and model predictive control (MPC) [25] have shortcomings in terms of accuracy and computation efficiency, respectively. The QP algorithm can strike a balance between computation efficiency and accuracy, especially when the objective function is quadratic, and the constraints are linear. It can be seen from the proposed optimal desired tension allocation model (18) and (19) that the objective function and constraints are quadratic and linear, respectively. Therefore, we chose the QP algorithm to achieve the optimal desired tension allocation of TS.*

3.3. Event-Triggered Neural Adaptive Distributed Cooperative Controllers for Tugs

Similar to the platform, we design a neural adaptive distributed cooperative controller for tugs.

Step 1: Firstly, the two errors of the ith ($i = 1,..,4$) tug is defined as follows:

$$\begin{cases} E_{1i} = \sum_{j\in\mathcal{N}_i} a_{ij}(\boldsymbol{e}_{1i} - \boldsymbol{e}_{1j}) + a_{i0}(\boldsymbol{e}_{1i}) \\ E_{2i} = \boldsymbol{v}_i - \boldsymbol{\vartheta}_i \end{cases} \tag{20}$$

where $\boldsymbol{e}_{1i} = \boldsymbol{\eta}_i - \boldsymbol{\eta}_0 - \eta_i^{t-v}$, a_{ij}, a_{i0} are adjacency matrices, $\mathcal{N}_i$ is the neighbor set for ith tug, and the details can be seen in preliminaries in [10,32]. The control law $\boldsymbol{\vartheta}_i \in R^3$ for the platform can be obtained as follows:

$$\boldsymbol{\vartheta}_i = \frac{\boldsymbol{J}^T(\psi)_i}{a_{id}}\left[-\boldsymbol{K}_{1i}\boldsymbol{E}_{1i} + \sum_{j\in\mathcal{N}_i} a_{ij}(\boldsymbol{J}^T(\psi)_i\boldsymbol{v}_i + \dot{\eta}_i^{t-v} - \dot{\eta}_j^{t-v}) - a_{i0}(\boldsymbol{J}^T(\psi)_0\boldsymbol{v}_0 + \dot{\eta}_i^{t-v})\right] \tag{21}$$

The $\bar{\boldsymbol{\vartheta}}_i$ can be obtained through first-order filter as follows:

$$k\dot{\bar{\boldsymbol{\vartheta}}}_i = \boldsymbol{\vartheta}_i - \bar{\boldsymbol{\vartheta}}_i, \quad \bar{\boldsymbol{\vartheta}}_i(0) = \boldsymbol{\vartheta}_i(0) \tag{22}$$

Based on the (20) and (3), we can obtain the derivative of (20) as follows:

$$\begin{cases} \dot{\boldsymbol{E}}_{1i} = a_{id}\boldsymbol{J}(\psi)_i \boldsymbol{v}_i - \sum\limits_{j\in\mathcal{N}_i} a_{ij}(\boldsymbol{J}(\psi)_j \boldsymbol{v}_j + \dot{\eta}_i^{t-v} - \dot{\eta}_j^{t-v}) - a_{i0}(\boldsymbol{J}(\psi)_0 \boldsymbol{v}_0 + \dot{\eta}_j^{t-v}) \\ \boldsymbol{M}_i \dot{\boldsymbol{E}}_{2i} = \boldsymbol{\tau}_i + \boldsymbol{d}_i - \boldsymbol{\tau}_h^i \end{cases} \tag{23}$$

where $\boldsymbol{d}_i = \boldsymbol{\tau}_w^i - \boldsymbol{D}_i \boldsymbol{v}_i - \boldsymbol{g}_i - \boldsymbol{M}_i \dot{\bar{\boldsymbol{\vartheta}}}_i$ includes total disturbances and uncertainties. The design process of the control effort $\tau_{i\_c}(t)$ of tugs are similar to the process of platform. The control effort $\tau_{i\_c}(t)$ are designed as follows:

$$\boldsymbol{\tau}_{i\_c}(t) = -\boldsymbol{K}_{2i} E_{2i} - \hat{\boldsymbol{d}}_i \tag{24}$$

where $\hat{\boldsymbol{d}}_i = \hat{\boldsymbol{\rho}}_i \boldsymbol{\varepsilon}_i E_{2i}$, $\boldsymbol{\tau}_{i\_c}(t) = \begin{bmatrix} \tau_{i\_c,1}(t) & \tau_{i\_c,2}(t) & \tau_{i\_c,3}(t) \end{bmatrix}$, $\boldsymbol{\rho}_i = diag(\rho_{i,1}, \rho_{i,2}, \rho_{i,3})$, $\hat{\boldsymbol{\rho}}_i = diag(\hat{\rho}_{i,1}, \hat{\rho}_{i,2}, \hat{\rho}_{i,3})$ is the estimation of $\boldsymbol{\rho}_i$, $\rho_{i,n} = \chi_{i,n}^2 (n = 1,2,3)$, $\boldsymbol{\varepsilon}_i = diag(\varepsilon_{i,1}, \varepsilon_{i,2}, \varepsilon_{i,3})$, with $\varepsilon_{i,n} = \xi_{i,n}^2 / (4\delta_{i,n}^2)$, and $\delta_{i,n}$ represents the positive constant. The update rate of $\hat{\rho}_n$ is as follows:

$$\dot{\hat{\rho}}_{i,n} = \beta_{i,n} \left\{ \varepsilon_{i,n} E_{2i,n} - \gamma_{i,n} \left[\hat{\rho}_{i,n} - \hat{\rho}_{i,n}(0) \right] \right\} \tag{25}$$

According to event-triggered control, the final control law is designed as follows:

$$\tau_{i,n}(t) = \tau_{i\_c,n}(t_{i,n}^s), \ \forall t \in [t_{i,n}^s, t_{i,n}^{s+1}), \ n{=}1,2,3 \tag{26}$$

where $\boldsymbol{\tau}_i(t) = \begin{bmatrix} \tau_{i,1}(t) & \tau_{i,2}(t) & \tau_{i,3}(t) \end{bmatrix}$, $t_{i,n}^s$ is the triggering time instant of the s-th event, and the triggering conditions are as follows:

$$\begin{cases} t_{i,n}^s = \inf \left\{ t \in R \,|\, |E_n| \geq \alpha_{i,n} \right\} \\ E_{i,n} = \boldsymbol{\tau}_{i\_c,n}(t_{i,n}^{s-1}) - \boldsymbol{\tau}_{i,n}(t_{i,n}^s) \end{cases} \tag{27}$$

where $\alpha_{i,n} \in R$, which satisfies $0 < \alpha_{i,n} < \bar{\alpha}_{i,n}$, with constants $\bar{\alpha}_{i,n}$. If the triggering condition of (27) is not met, $\tau_{i,n}(t)$ remains constant $\tau_{i\_c,n}(t_{i,n}^{s-1})$. When triggering condition (27) is met, the current triggering moment is marked as $t_{i,n}^s$, and control input $\tau_{i,n}(t)$ will change to $\tau_{i\_c,n}(t_n^s)$.

Based on (23)–(25) and defining $\tilde{\rho}_{i,n} = \hat{\rho}_{i,n} - \rho_{i,n}$, we obtain the following:

$$\begin{cases} \dot{\boldsymbol{E}}_{1i} = -K_{1i}\boldsymbol{E}_{1i} + \boldsymbol{J}(\boldsymbol{\psi})_i \left(\boldsymbol{E}_{2i} + \boldsymbol{q}_i \right) \\ M_i \dot{\boldsymbol{E}}_{2i} = -\boldsymbol{K}_{2i}\boldsymbol{E}_{2i} - \hat{\boldsymbol{\rho}}_i \boldsymbol{\varepsilon}_i \boldsymbol{E}_{2i} + \boldsymbol{d}_i \\ \dot{\tilde{\rho}}_{i,n} = \beta_{i,n} \left\{ \varepsilon_{i,n} E^2{}_{2i,n} - \gamma_{i,n} \left[\hat{\rho}_{i,n} - \hat{\rho}_{i,n}(0) \right] \right\} \end{cases} \tag{28}$$

where $\boldsymbol{q}_i = \bar{\boldsymbol{\vartheta}}_i - \boldsymbol{\vartheta}_i$.

3.4. Stability Analysis

Theorem 1. *For the system errors (17) and (28) of the platform and tugs with unknown disturbances and uncertainties, and according to Assumptions 1–3, the proposed control scheme, composed of dynamics control law (15) and (24) and the update rate (16) and (25), can achieve the control objectives of this paper. Additionally, in the closed-loop system, all signals of the TS are ultimately uniformly bounded.*

Proof. Based on the errors discussed above, we established the following Lyapunov function as follows:

$$V=\frac{1}{2}\left(\boldsymbol{E}_{10}^{T}\boldsymbol{E}_{10}+\boldsymbol{E}_{20}^{T}\boldsymbol{M}\boldsymbol{E}_{20}+\frac{1}{\beta_{0,n}}\sum_{n=1}^{3}\tilde{\rho}_{0,n}^{2}\right)+\frac{1}{2}\sum_{i=1}^{4}\left(\boldsymbol{E}_{1i}^{T}\boldsymbol{E}_{1i}+\boldsymbol{E}_{2i}^{T}\boldsymbol{M}\boldsymbol{E}_{2i}+\frac{1}{\beta_{i,n}}\sum_{n=1}^{3}\tilde{\rho}_{i,n}^{2}\right) \quad (29)$$

The derivative of (29) as follows:

$$\begin{aligned}\dot{V}=&\boldsymbol{E}_{10}^{T}\dot{\boldsymbol{E}}_{10}+\boldsymbol{E}_{20}^{T}\boldsymbol{M}\dot{\boldsymbol{E}}_{20}+\sum_{n=1}^{3}\tilde{\rho}_{0,n}\dot{\tilde{\rho}}_{0,n}+\sum_{i=1}^{4}\left(\boldsymbol{E}_{1i}^{T}\dot{\boldsymbol{E}}_{1i}+\boldsymbol{E}_{2i}^{T}\boldsymbol{M}\dot{\boldsymbol{E}}_{2i}+\sum_{n=1}^{3}\tilde{\rho}_{i,n}\dot{\tilde{\rho}}_{i,n}\right)\\
=&\boldsymbol{E}_{10}^{T}\left[-K_{10}\boldsymbol{E}_{10}+\boldsymbol{J}(\boldsymbol{\psi})_{0}\left(\boldsymbol{E}_{20}+\boldsymbol{q}_{0}\right)\right]+\boldsymbol{E}_{20}^{T}\left(-\boldsymbol{K}_{20}\boldsymbol{E}_{20}-\hat{\boldsymbol{\rho}}_{0}\boldsymbol{\varepsilon}_{0}\boldsymbol{E}_{20}+\boldsymbol{d}_{0}\right)\\
&+\sum_{n=1}^{3}\tilde{\rho}_{0,n}\left\{\varepsilon_{0,n}E^{2}{}_{20,n}-\gamma_{0,n}\left[\hat{\rho}_{0,n}-\hat{\rho}_{0,n}(0)\right]\right\}\\
&+\sum_{i=1}^{4}\begin{Bmatrix}\left\{\boldsymbol{E}_{1i}^{T}\left(-K_{1i}\boldsymbol{E}_{1i}+\boldsymbol{J}(\boldsymbol{\psi})_{i}\left(\boldsymbol{E}_{2i}+\boldsymbol{q}_{i}\right)\right)+\boldsymbol{E}_{2i}^{T}\left(-\boldsymbol{K}_{2i}\boldsymbol{E}_{2i}-\hat{\boldsymbol{\rho}}_{i}\boldsymbol{\varepsilon}_{i}\boldsymbol{E}_{2i}+\boldsymbol{d}_{i}\right)\right.\\
+\sum_{n=1}^{3}\tilde{\rho}_{i,n}\left\{\varepsilon_{i,n}E^{2}{}_{2i,n}-\gamma_{i,n}\left[\hat{\rho}_{i,n}-\hat{\rho}_{i,n}(0)\right]\right\}\end{Bmatrix}\\
=&-\boldsymbol{E}_{10}^{T}K_{10}\boldsymbol{E}_{10}+\boldsymbol{E}_{10}^{T}\boldsymbol{J}(\boldsymbol{\psi})_{0}\left(\boldsymbol{E}_{20}+\boldsymbol{q}_{0}\right)+-\boldsymbol{E}_{20}^{T}\boldsymbol{K}_{20}\boldsymbol{E}_{20}+\boldsymbol{E}_{20}^{T}\left(-\hat{\boldsymbol{\rho}}_{0}\boldsymbol{\varepsilon}_{0}\boldsymbol{E}_{20}+\boldsymbol{d}_{0}\right)\\
&+\sum_{n=1}^{3}\tilde{\rho}_{0,n}\varepsilon_{0,n}E^{2}{}_{20,n}-\sum_{n=1}^{3}\tilde{\rho}_{0,n}\gamma_{0,n}\left[\hat{\rho}_{0,n}-\hat{\rho}_{0,n}(0)\right]\\
&+\sum_{i=1}^{4}\begin{Bmatrix}\left\{-\boldsymbol{E}_{1i}^{T}K_{1i}\boldsymbol{E}_{1i}+\boldsymbol{E}_{1i}^{T}\boldsymbol{J}(\boldsymbol{\psi})_{i}\left(\boldsymbol{E}_{2i}+\boldsymbol{q}_{i}\right)+-\boldsymbol{E}_{2i}^{T}\boldsymbol{K}_{2i}\boldsymbol{E}_{2i}+\boldsymbol{E}_{2i}^{T}\left(-\hat{\boldsymbol{\rho}}_{i}\boldsymbol{\varepsilon}_{i}\boldsymbol{E}_{2i}+\boldsymbol{d}\right)_{i}\right.\\
+\sum_{n=1}^{3}\tilde{\rho}_{i,n}\varepsilon_{i,n}E^{2}{}_{2i,n}-\sum_{n=1}^{3}\tilde{\rho}_{i,n}\gamma_{i,n}\left[\hat{\rho}_{i,n}-\hat{\rho}_{i,n}(0)\right]\end{Bmatrix}\end{aligned} \quad (30)$$

According to references [33], $\boldsymbol{q}_0$ and $\boldsymbol{q}_i$ are bounded, such that $\|\boldsymbol{q}_0\|\le\overline{\boldsymbol{q}}_0$, $\|\boldsymbol{q}_i\|\le\overline{\boldsymbol{q}}_i$, where $\overline{\boldsymbol{q}}_0$ and $\overline{\boldsymbol{q}}_i$ are constants. Based on the Young's inequality, we can obtain the inequalities as follows:

$$\begin{cases}\boldsymbol{E}_{10}^{T}\boldsymbol{J}(\boldsymbol{\psi})_{0}\left(\boldsymbol{E}_{20}+\boldsymbol{q}_{0}\right)\le\sigma_{0}\boldsymbol{E}_{10}^{T}\boldsymbol{E}_{10}+\dfrac{1}{2\sigma_{0}}\boldsymbol{E}_{20}^{T}\boldsymbol{E}_{20}+\dfrac{1}{2\sigma_{0}}\overline{\boldsymbol{q}}_{0}^{2}\\
\boldsymbol{E}_{1i}^{T}\boldsymbol{J}(\boldsymbol{\psi})_{i}\left(\boldsymbol{E}_{2i}+\boldsymbol{q}_{i}\right)\le\sigma_{i}\boldsymbol{E}_{1i}^{T}\boldsymbol{E}_{1i}+\dfrac{1}{2\sigma_{i}}\boldsymbol{E}_{2i}^{T}\boldsymbol{E}_{2i}+\dfrac{1}{2\sigma_{i}}\overline{\boldsymbol{q}}^{2}\\
\boldsymbol{E}_{20}^{T}\left(-\hat{\boldsymbol{\rho}}_{0}\boldsymbol{\varepsilon}_{0}\boldsymbol{E}_{20}+\boldsymbol{d}_{0}\right)\le-\boldsymbol{E}_{20}^{T}\hat{\boldsymbol{\rho}}_{0}\boldsymbol{\varepsilon}_{0}\boldsymbol{E}_{20}+\displaystyle\sum_{n=1}^{3}\left(\frac{\tilde{\rho}_{0,n}E_{20,n}^{2}\xi^{2}{}_{0,n}}{4\gamma_{0,n}^{2}}+\gamma_{0,n}^{2}\right)\\
\qquad\le\displaystyle\sum_{n=1}^{3}\left(\frac{\tilde{\rho}_{0,n}E_{20,n}^{2}\xi^{2}{}_{0,n}}{4\gamma_{0,n}^{2}}+\gamma^{2}{}_{0,n}\right)\\
\boldsymbol{E}_{2i}^{T}\left(-\hat{\boldsymbol{\rho}}_{i}\boldsymbol{\varepsilon}_{i}\boldsymbol{E}_{2i}+\boldsymbol{d}_{i}\right)\le-\boldsymbol{E}_{2i}^{T}\hat{\boldsymbol{\rho}}_{i}\boldsymbol{\varepsilon}_{i}\boldsymbol{E}_{2i}+\displaystyle\sum_{n=1}^{3}\left(\frac{\tilde{\rho}_{i,n}E_{2i,n}^{2}\xi_{i,n}^{2}}{4\gamma_{i,n}^{2}}+\gamma_{i,n}^{2}\right)\\
\qquad\le\displaystyle\sum_{n=1}^{3}\left(\frac{\tilde{\rho}_{i,n}E_{2i,n}^{2}\xi_{i,n}^{2}}{4\gamma_{i,n}^{2}}+\gamma_{i,n}^{2}\right)\\
-\tilde{\rho}_{0,n}\left[\hat{\rho}_{0,n}-\hat{\rho}_{0,n}(0)\right]\le-\dfrac{1}{2}\tilde{\rho}_{0,n}^{2}+\dfrac{1}{2}\left[\rho_{0,n}-\hat{\rho}_{0,n}\left(0\right)\right]^{2}\\
-\tilde{\rho}_{i,n}\left[\hat{\rho}_{i,n}-\hat{\rho}_{i,n}(0)\right]\le-\dfrac{1}{2}\tilde{\rho}_{i,n}^{2}+\dfrac{1}{2}\left[\rho_{i,n}-\hat{\rho}_{i,n}\left(0\right)\right]^{2}\end{cases} \quad (31)$$

where σ_0 and σ_i are constant. By substituting (31) into (30), we can obtain the follow inequality.

$$
\begin{aligned}
\dot{V} \le & -\boldsymbol{E}_{10}^{T}K_{10}\boldsymbol{E}_{10}+\sigma_0\boldsymbol{E}_{10}^{T}\boldsymbol{E}_{10}+\frac{1}{2\sigma_0}\boldsymbol{E}_{20}^{T}\boldsymbol{E}_{20}-\boldsymbol{E}_{20}^{T}K_{20}\boldsymbol{E}_{20} \\
& -\sum_{n=1}^{3}\frac{\gamma_{0,n}\tilde{\rho}_{0,n}^{2}}{2}+\frac{1}{2\sigma_0}\overline{\boldsymbol{q}}_0^{2}+\sum_{n=1}^{3}\beta_{0,n}^{2}+\sum_{n=1}^{3}\frac{\gamma_{0,n}}{2}\left[\rho_{0,n}-\hat{\rho}_{0,n}(0)\right]^{2} \\
& +\sum_{i=1}^{4}\left\{-\boldsymbol{E}_{1i}^{T}K_{1i}\boldsymbol{E}_{1i}+\sigma_i\boldsymbol{E}_{1i}^{T}\boldsymbol{E}_{1i}+\frac{1}{2\sigma_i}\boldsymbol{E}_{2i}^{T}\boldsymbol{E}_{2i}-\boldsymbol{E}_{2i}^{T}K_{2i}\boldsymbol{E}_{2i}\right. \\
& \left.-\sum_{n=1}^{3}\frac{\gamma_{i,n}\tilde{\rho}_{i,n}^{2}}{2}+\frac{1}{2\sigma_i}\overline{\boldsymbol{q}}_i^{2}+\sum_{n=1}^{3}\beta_{i,n}^{2}+\sum_{n=1}^{3}\frac{\gamma_{i,n}}{2}\left[\rho_{i,n}-\hat{\rho}_{i,n}(0)\right]^{2}\right\} \\
\le & -\left[\lambda_{\min}(K_{10})-\sigma_0\right]\|\boldsymbol{E}_{10}\|^{2}-\left[\lambda_{\min}(K_{20})-\frac{1}{2\sigma_0}\right]\|\boldsymbol{E}_{20}\|^{2}-\frac{\gamma_{0,n}}{2}\sum_{n=1}^{3}\tilde{\rho}_{0,n}^{2} \\
& +\sum_{n=1}^{3}\frac{1}{2\sigma_0}\overline{\boldsymbol{q}}_0^{2}+\sum_{n=1}^{3}\beta_{0,n}^{2}+\sum_{n=1}^{3}\frac{\gamma_{0,n}}{2}\left[\rho_{0,n}-\hat{\rho}_{0,n}(0)\right]^{2} \\
& +\sum_{i=1}^{4}\left\{-\left[\lambda_{\min}(K_{1i})-\sigma_i\right]\|\boldsymbol{E}_{1i}\|^{2}-\left[\lambda_{\min}(K_{2i})-\frac{1}{2\sigma_i}\right]\|\boldsymbol{E}_{2i}\|^{2}-\frac{\gamma_{i,n}}{2}\sum_{n=1}^{3}\tilde{\rho}_{i,n}^{2}\right. \\
& \left.+\sum_{n=1}^{3}\frac{1}{2\sigma_i}\overline{\boldsymbol{q}}_i^{2}+\sum_{n=1}^{3}\beta_{i,n}^{2}+\sum_{n=1}^{3}\frac{\gamma_{i,n}}{2}\left[\rho_{i,n}-\hat{\rho}_{i,n}(0)\right]^{2}\right\} \\
\le & -c_1\frac{1}{2}\left(\boldsymbol{E}_{10}^{T}\boldsymbol{E}_{10}+\boldsymbol{E}_{20}^{T}\boldsymbol{M}\boldsymbol{E}_{20}+\frac{1}{\beta_{0,n}}\sum_{n=1}^{3}\tilde{\rho}_{0,n}^{2}\right)+c_2 \\
& -c_3\frac{1}{2}\sum_{i=1}^{4}\left(\boldsymbol{E}_{1i}^{T}\boldsymbol{E}_{1i}+\boldsymbol{E}_{2i}^{T}\boldsymbol{M}\boldsymbol{E}_{2i}+\frac{1}{\beta_{i,n}}\sum_{n=1}^{3}\tilde{\rho}_{i,n}^{2}\right)+c_4 \\
\le & -cV+c_2+c_4
\end{aligned}
\tag{32}
$$

where $c=\min(c_1,\ c_3)$, $c_1=2\min\left\{\lambda_{\min}(K_{1i})-\sigma_i,\ \dfrac{\lambda_{\min}(K_{2i})-\dfrac{1}{2\sigma_i}}{\lambda_{\max}(K_{2i})},\ \dfrac{\beta_{i,n}\gamma_{i,n}}{2}\right\}$,

$c_2=\sum_{n=1}^{3}\dfrac{1}{2\sigma_0}\overline{\boldsymbol{q}}_0^{2}+\sum_{n=1}^{3}\beta_{0,n}^{2}+\sum_{n=1}^{3}\dfrac{\gamma_{0,n}}{2}\left[\rho_{0,n}-\hat{\rho}_{0,n}(0)\right]^{2}$,

$c_3=2\min\left\{\lambda_{\min}(K_{1i})-\sigma_i,\ \dfrac{\lambda_{\min}(K_{2i})-\dfrac{1}{2\sigma_i}}{\lambda_{\max}(K_{2i})},\ \dfrac{\beta_{i,n}\gamma_{i,n}}{2}\right\}$,

$c_2=\sum_{n=1}^{3}\dfrac{1}{2\sigma_i}\overline{\boldsymbol{q}}_i^{2}+\sum_{n=1}^{3}\beta_{i,n}^{2}+\sum_{n=1}^{3}\dfrac{\gamma_{i,n}}{2}\left[\rho_{i,n}-\hat{\rho}_{i,n}(0)\right]^{2}$. $\lambda_{\min}$ and $\lambda_{\max}$ represent the minimum and maximum eigenvalues of the matrix, respectively. $c_2+c_4>0$ and $c>0$ can be obtained by choosing parameters.

Further, the closed-loop system is uniformly ultimately bounded. Finally, Theorem 1 is proven.

Theorem 2. In this paper, the fixed-threshold event-triggering mechanisms (15), (16), (26), and (27) can effectively prevent Zeno behavior, and the time intervals $t_{0,n}^{s}-t_{0,n}^{s-1}$ and $t_{i,n}^{s}-t_{i,n}^{s-1}$ have lower bound $\underline{t}$, where $\underline{t}$ is a positive constant.

Proof. Based on (16), the derivative of E_{0n} as follows:

$$
\dot{E}_{0,n}=sign\left(E_{0,n}\right)\dot{E}_{0,n}\le\left|\boldsymbol{\tau}_{0\_c}\right|,\ \forall t\in[t_{0,n}^{s-1},t_{0,n}^{s}]
\tag{33}
$$

According to (13), the derivative of $\boldsymbol{\tau}_{0\_c}$ with respect to $\dot{\boldsymbol{\tau}}_{0\_c}$ is as follows:

$$\dot{\tau}_{0\_c,n}(t) = -K_{20,n}\dot{E}_{20,n} - \dot{\hat{\rho}}_{0,n}\varepsilon_{0,n}E_{20,n} - \hat{\rho}_{0,n}\dot{\varepsilon}_{0,n}E_{20,n} - \hat{\rho}_{0,n}\varepsilon_{0,n}\dot{E}_{20,n} \tag{34}$$

According to Theorem 1, $\dot{E}_{20,n}$ and $\dot{\hat{\rho}}_{0,n}$ are bounded. Based on Lemma 1, $h(\delta)$ and first derivative $\dot{h}(\delta)$ are bounded, and subsequently, $\dot{\boldsymbol{\varepsilon}}_{0,n}$ is bounded as well. Therefore, there exists a positive number $\varpi_{0,n}$ such that $\left|\dot{E}_{0,n}\right| \le \varpi_{0,n}$.

$$E_{0,n}\left(t_{0,n}^{s-1}\right) = 0,\ \lim_{t\to t_{0,n}^{s}}\left|E_{0,n}(t)\right| = \alpha_0 \tag{35}$$

Based on (35), the time interval has lower bound $\underline{t}$, where $\underline{t} \ge \min\left\{\alpha_0/\varpi_{0,n}\right\}$. Therefore, the proposed ETC method can avoid Zeno behavior. Similarly, the above proof also applies to the neural adaptive distributed cooperative controller for tugs.

Theorem 2 is proven. □

4. Simulation Results and Analysis

In this section, we employ the towing system (TS) [10] to validate the effectiveness of the proposed control method. To show the performance of the designed control method, our simulations and experiments were conducted using MATLAB 2023b and Windows 11. The parameters of the unactuated platform and four tugs of the TS can be seen in [10] and Table 1. The following desired trajectory can only be gained by the platform.

$$\begin{cases} x(t) = 0.2t \\ y(t) = 200sin(0.001t) \end{cases} \tag{36}$$

In practice, the TS usually navigates in a moderate sea condition. However, it is also essential to consider its reliability under different conditions. Therefore, this paper introduced the following two types of unknown disturbances [34]:

Case 1. Based on Ref. [35], the unknown disturbances τ_w and the model uncertainties g of moderate sea conditions are designed as follows:

$$\begin{cases} \tau_w^i = 10^3\left[5\sin(t), 5\sin(t), 5\sin(t)\right]^T, i = 1,2,3,4 \\ g_i = 10^3\left[0.3u_i v_i^2 + 0.4v_i^2 r_i, 0.1u_i v_i, 0.2u_i r_i^2 + 0.3u_i r_i v_i\right]^T \\ \tau_w^0 = 10^4\left[5\sin(t), 5\sin(t), 5\sin(t)\right]^T \\ g_0 = 10^4\left[0.3u_0 v_0^2 + 0.4v_0^2 r_0, 0.1u_0 v_0, 0.2u_0 r_0^2 + 0.3u_0 r_0 v_0\right]^T \end{cases} \tag{37}$$

Case 2. The unknown disturbances τ_w and the model uncertainties g of adverse sea conditions are designed as follows:

$$\begin{cases} \tau_w^i = 10^5\left[5\sin(t), 5\sin(t), 5\sin(t)\right]^T, i = 1,2,3,4 \\ g_i = 10^5\left[0.3u_i v_i^2 + 0.4v_i^2 r_i, 0.1u_i v_i, 0.2u_i r_i^2 + 0.3u_i r_i v_i\right]^T \\ \tau_w^0 = 10^6\left[5\sin(t), 5\sin(t), 5\sin(t)\right]^T \\ g_0 = 10^6\left[0.3u_0 v_0^2 + 0.4v_0^2 r_0, 0.1u_0 v_0, 0.2u_0 r_0^2 + 0.3u_0 r_0 v_0\right]^T \end{cases} \tag{38}$$

Table 1. Initial positions and initial velocities of the platform and four tugs.

The Towing System	Initial Positions	Initial Velocities
The offshore platform	$\eta_0 = [0,0,0^\circ]^T$	$v_0 = [0,0,0(\mathrm{rad/s})]^T$
The first tug	$\eta_1 = [271,-167,0^\circ]^T$	$v_1 = [0,0,0(\mathrm{rad/s})]^T$
The second tug	$\eta_2 = [271,167,0^\circ]^T$	$v_2 = [0,0,0(\mathrm{rad/s})]^T$

The third tug	$\eta_3 = [-271, 167, 180^\circ]^T$	$v_3 = [0, 0, 0(\text{rad/s})]^T$
The fourth tug	$\eta_4 = [-271, -167, 180^\circ]^T$	$v_4 = [0, 0, 0(\text{rad/s})]^T$

Considering that symmetrically distributed tugs can better coordinate the towing force on the platform, we use the same transformation matrix B_0 with [10]. The parameters are as follows: $\theta_1 = 330^\circ$, $\theta_2 = 30^\circ$, $\theta_3 = 150^\circ$, $\theta_4 = 210^\circ$; $(l_{x1}, l_{y1}) = (55m, -42m)$, $(l_{x2}, l_{y2}) = (55m, 42m)$, $(l_{x3}, l_{y3}) = (-55m, 42m)$, $(l_{x4}, l_{y4}) = (-55m, -42m)$; $\phi_1 = \phi_3 = 150^\circ$, $\phi_2 = \phi_4 = 210^\circ$.

Based on the Theorem 1, we design the parameters of the proposed control scheme by trial and error. And the final designed parameters are as follows: $\boldsymbol{K}_{10} = 0.55 I_3$, $\boldsymbol{K}_{20} = 10^6 I_3$, $\boldsymbol{K}_{1i} = 5 I_3$, $\boldsymbol{K}_{2i} = diag\left(1e^5, 1e^6, 1e^7\right)$, $\beta_{01} = \beta_{02} = 0.02$, $\beta_{03} = 10$, $\beta_{i1} = \beta_{i2} = 2e^{-3}$, $\beta_{i3} = 0.1$, $\gamma_{01} = \gamma_{02} = 1e^{-3}$, $\gamma_{03} = 1e^{-4}$, $\gamma_{i1} = \gamma_{i2} = 4e^{-4}$, $\gamma_{i3} = 8e^{-3}$, $\delta_{01} = \delta_{02} = 500$, $\delta_{03} = 50$, $\delta_{i1} = \delta_{i2} = 800$, $\delta_{i3} = 50$, $\hat{\boldsymbol{\rho}}_0(0) = \hat{\boldsymbol{\rho}}_i(0) = 0$, $\alpha_{0,1} = \alpha_{0,2} = 1e^4 N$, $\alpha_{0,3} = 1e^6 N$, $\alpha_{i,1} = \alpha_{i,2} = 1e^5 N$, $\alpha_{i,3} = 1e^7 N$, $\rho_i = 0.08$.

To validate the advantages of the proposed MLP-based adaptive RBFNN, the single-hidden-layer neural network (SHLNN) is introduced as follows:

$$\hat{\rho}_i(t) = \hat{W}_i^T h(\chi_i) \tag{39}$$

where $\chi_i = [1, \nu_i^T, \dot{\eta}_i^T, \psi_i]^T$ is the input vector for the single-hidden-layer neural network, $\hat{W}_i$ is the estimated weight vector, and $h(\chi_i) = \dfrac{1}{1+e^{-\chi_i}}$ is the basis function of the neural network.

The adaptive update rule for $\hat{W}_i$ are designed as follows:

$$\dot{\hat{W}}_i = \sigma_i \left(h(\chi_i) E_i^T k_i \bar{M}_i^{-1}(\eta_i) - k_{wi} \hat{W}_i \right) \tag{40}$$

where σ_i is the gain parameters.

The simulation results are as follows:

Figure 4 describes the three adaptive learning parameters designed for the platform and tugs. It is evident from Figure 4 that the adaptive learning parameters stabilize at around 50 s. Figures 5 and 6 demonstrate that the MLP-based adaptive RBFNNs can effectively approximate the total disturbances and uncertainties of the TS, which can improve the robustness of the TS. By comparing the curves of MLP-based adaptive RBFNN and SHLNN in Figures 5 and 6, it is evident that both methods can achieve similar approximation results for the total disturbances and uncertainties around 70 s. This means that the MLP-based adaptive RBFNN can reduce the design and computational burden caused by numerous learning parameters without compromising the performance.

Figures 7 and 8 illustrate the control forces of the tugs under ETC in **Case 1** and **Case 2**. Clearly, the tugs' control forces are not continuously changing, it only adjusts when the control input error exceeds the predefined fixed threshold. Although there are some fluctuations in the control forces under **Case 2**, they remain within an acceptable range. This means that the control scheme proposed in our paper has good robustness to different sea conditions. To further validate the effectiveness of ETC, the execution frequency and inter-execution time $(t_{n+1}^s - t_n^s)$, $s = 0, 1, 2\ldots$, are given for the fourth tug under the two controllers (ETC and CTC). The comparison of the execution frequency in Figure 9 demonstrates that the designed ETC mechanism can effectively reduce the execution frequency of the tugs' thrusters and the communication burden within the TS. Furthermore, it can be seen from the detailed enlarged view of Figure 10 that the minimum inter-execution time is greater than 0 s, which validates that the proposed scheme can avoid Zeno behavior.

Figures 11 and 12 show the trajectories of the TS tracking straight and curved predetermined trajectories, respectively. It can be seen from Figures 11 and 12 that the platform can track the arbitrary predetermined trajectory well under the towing of tugs. Figures 13–15 show the position error curves of the platform and tugs under the two controllers (ETC and CTC). Figure 16 shows the deviations in the tugs' positions under two controllers. It can be seen from the first two items of Figure 16 that the north and east deviations are both within a small range. And the third item of Figure 16 shows that the heading deviations can converge to a small neighborhood within 100 s. Therefore, although there are slight oscillations of the proposed controller under the ETC, the overshoot and the convergence time remain basically consistent with those under CTC. Overall, Figures 11–16 show that the designed ETC mechanism can effectively reduce the thruster execution frequency and the communication burden with minimal impact on the performance of controller.

Figures 17 and 18 represent the horizontal lengths and horizontal tensions of towlines, which demonstrate that the length variation in towlines are relatively small and consistent with the horizontal tension variation in the towlines under the ETC mechanism. The relatively small length change in towlines can guarantee the trajectory-tracking performance of the platform. Based on the configuration of the TS in Figure 9 and the desired trajectory of the platform, the second and third tugs should provide the main drag forces at the initial stage, which is consistent with the horizontal length of towlines shown in Figure 13.

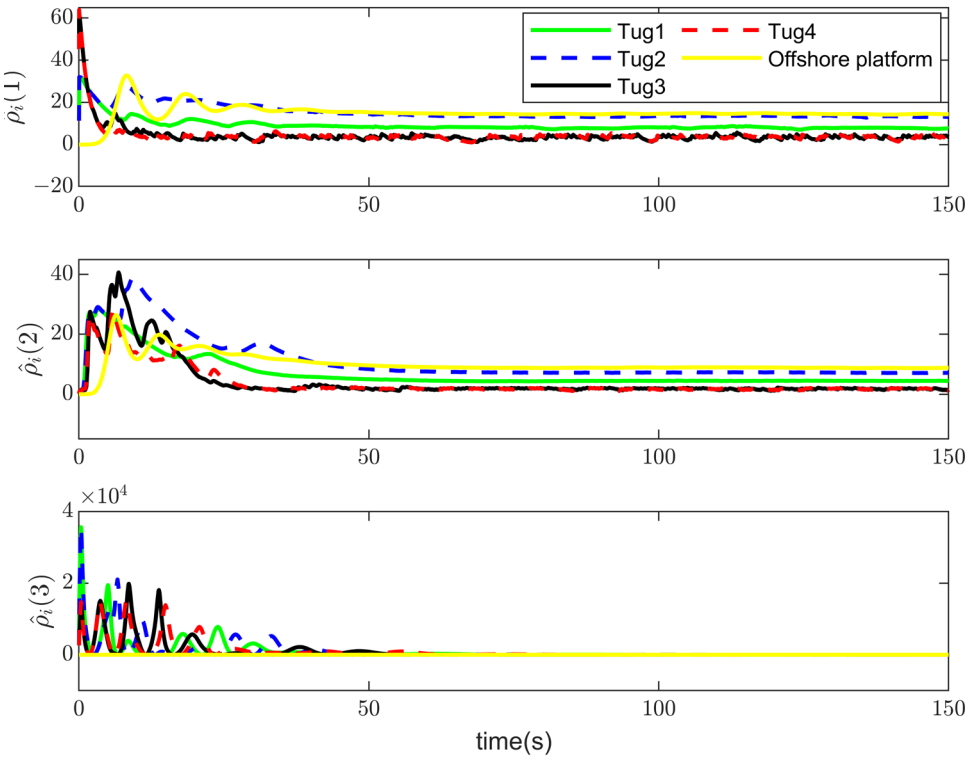

Figure 4. The adaptive learning parameters of the RBFNN for the TS in **Case 1**.

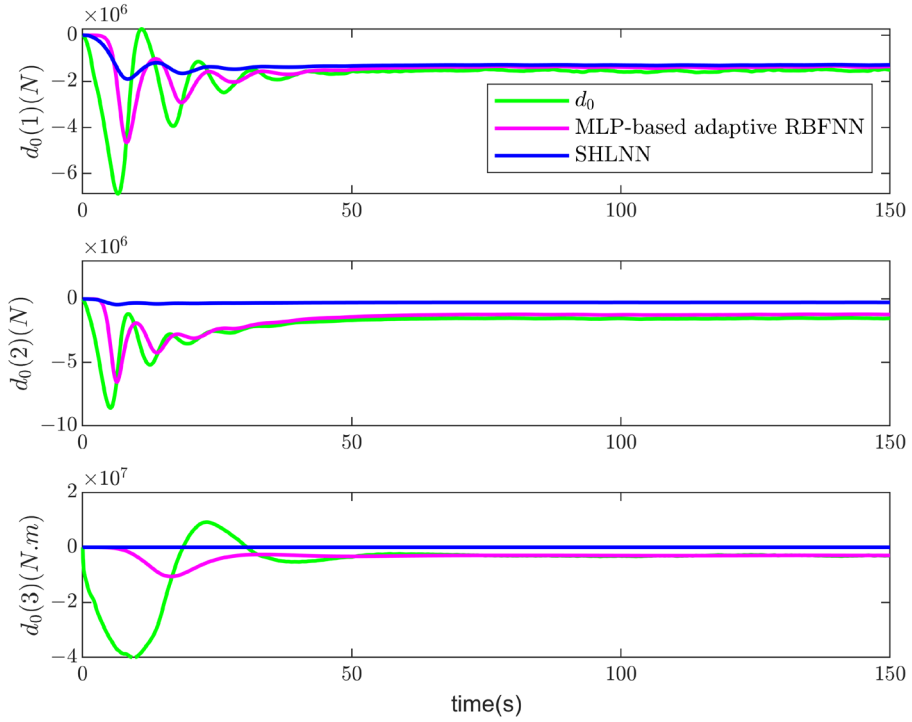

Figure 5. The actual total disturbances and uncertainties $\boldsymbol{d}_0$ of the platform and their estimation using MLP-based adaptive RBFNN and SHLNN in **Case 1.**

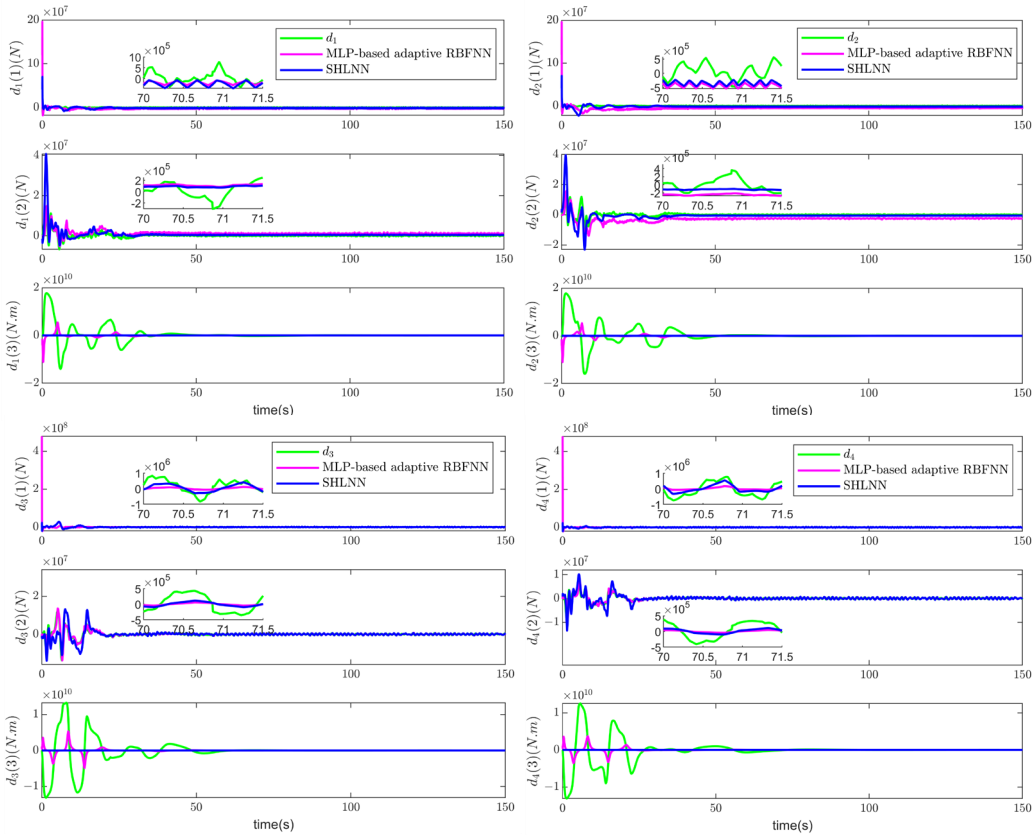

Figure 6. The actual total disturbances and uncertainties $\boldsymbol{d}_i$ of the tugs and their estimation using MLP-based adaptive RBFNN and SHLNN in **Case 1**.

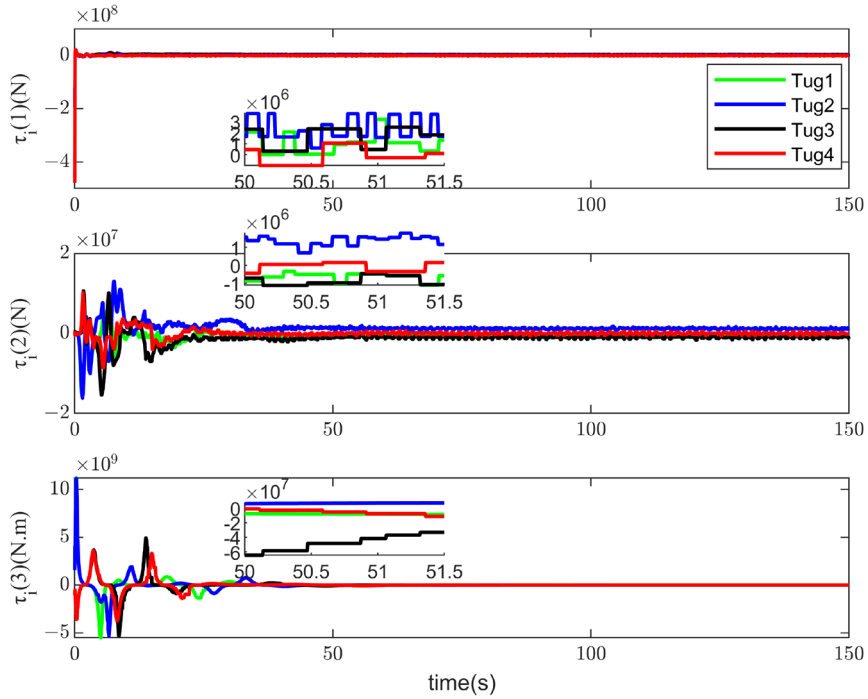

Figure 7. The control forces of the tugs under ETC in **Case 1**.

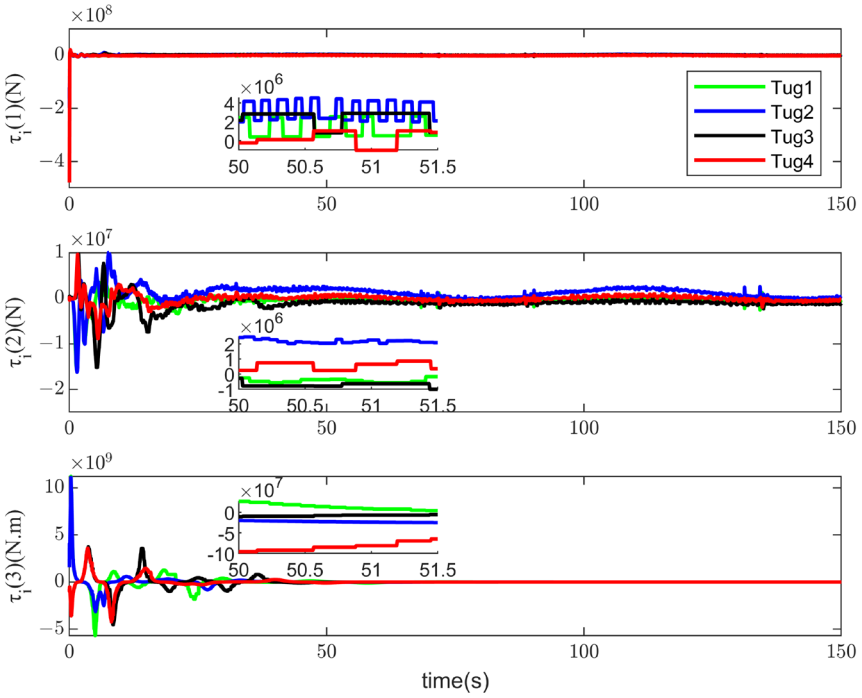

Figure 8. The control forces of the tugs under ETC in **Case 2**.

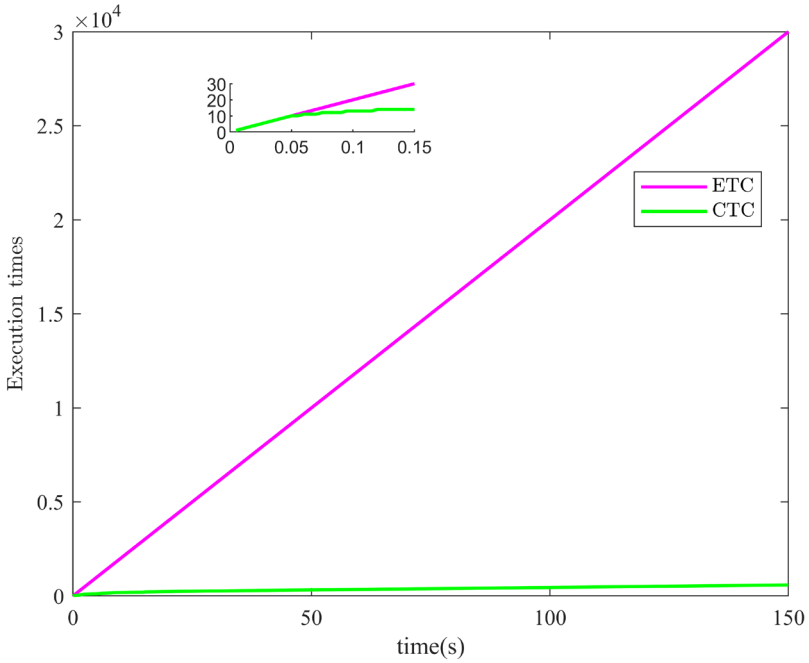

Figure 9. The execution times under the two controllers (ETC and CTC) in **Case 1**.

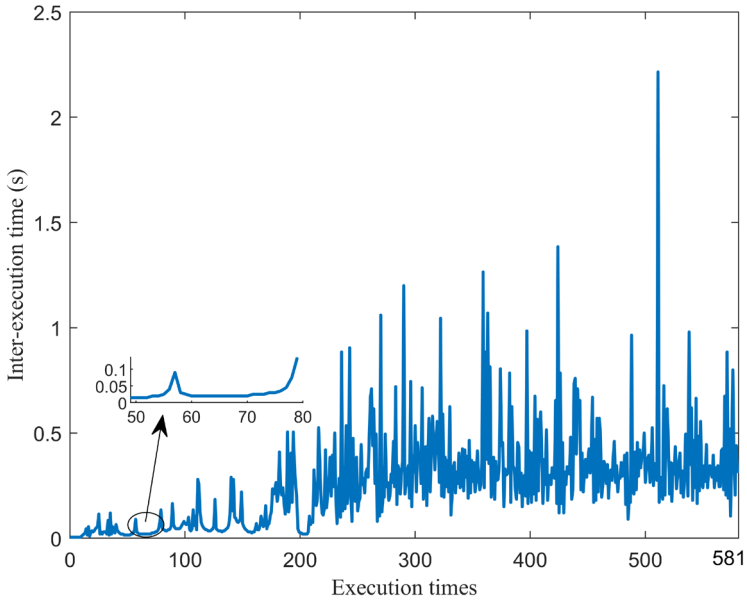

Figure 10. The inter-execution time of event-triggered neural adaptive cooperative controller in **Case 1**.

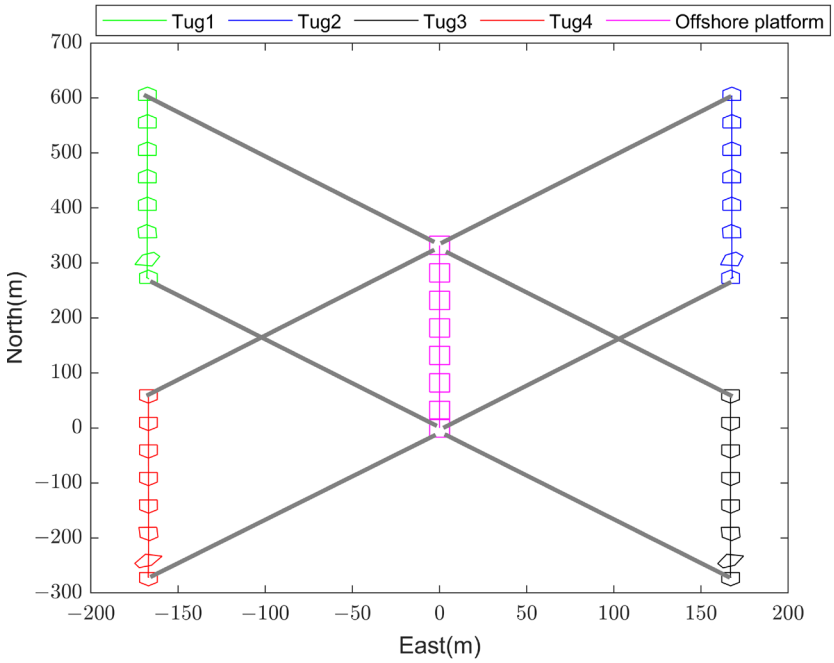

Figure 11. Trajectories of the offshore platform and tugs in the TS tracking straight predetermined trajectory in **Case 1**.

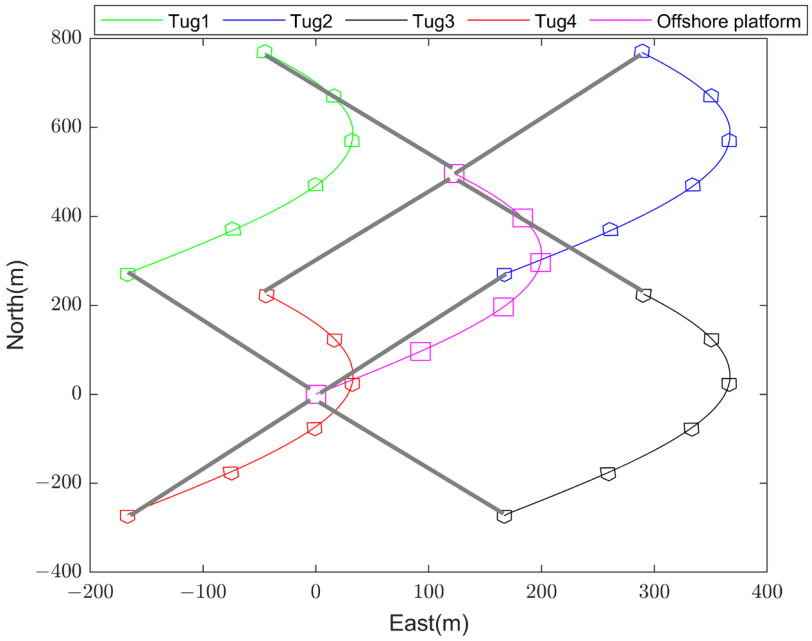

Figure 12. Trajectories of the offshore platform and tugs in the TS tracking curved predetermined trajectory in **Case 1.**

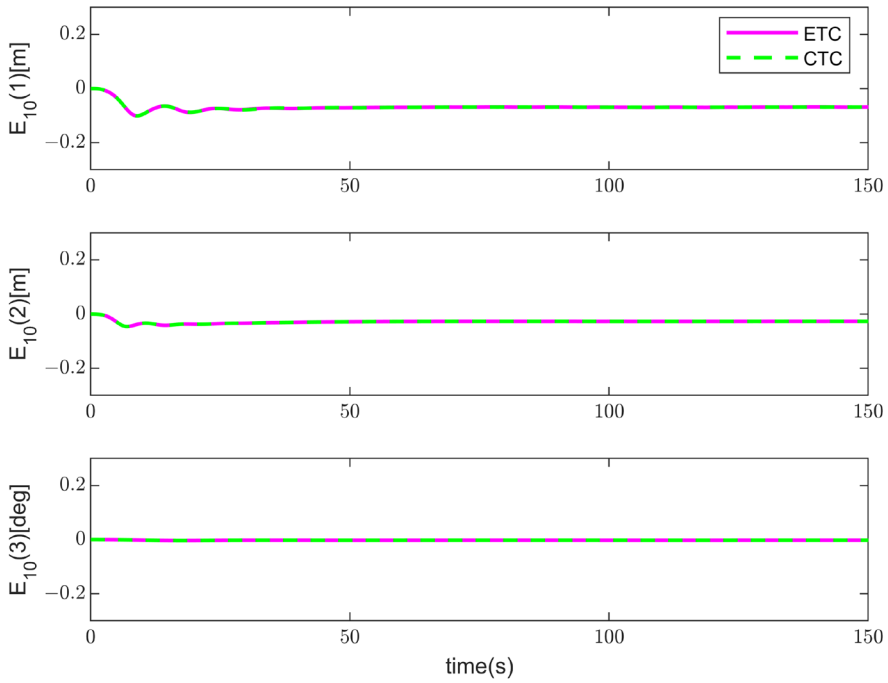

Figure 13. The position error curves of the platform under the two controllers (ETC and CTC) in **Case 1**.

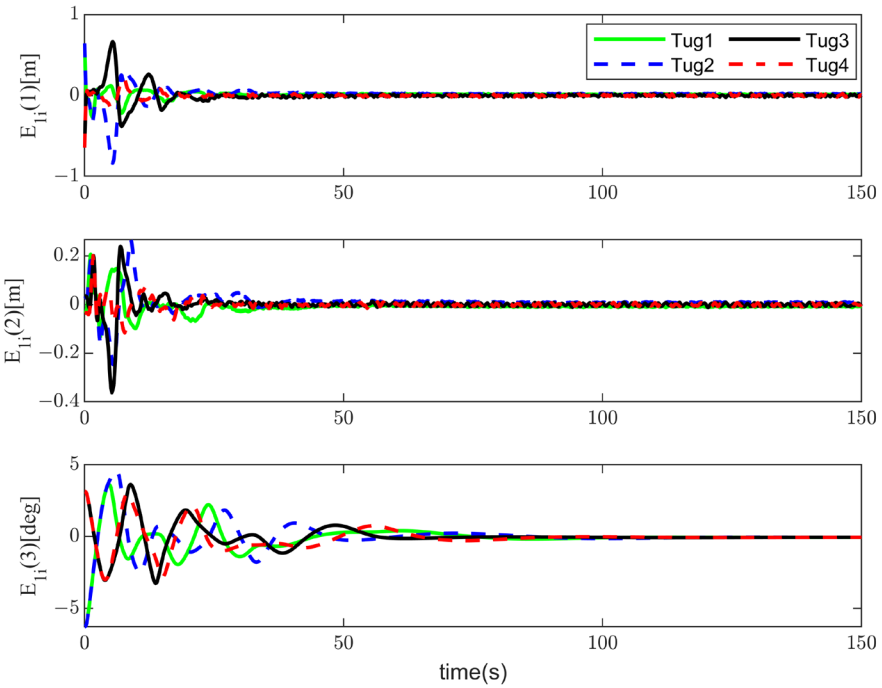

Figure 14. The position error curves of the tugs under ETC in **Case 1**.

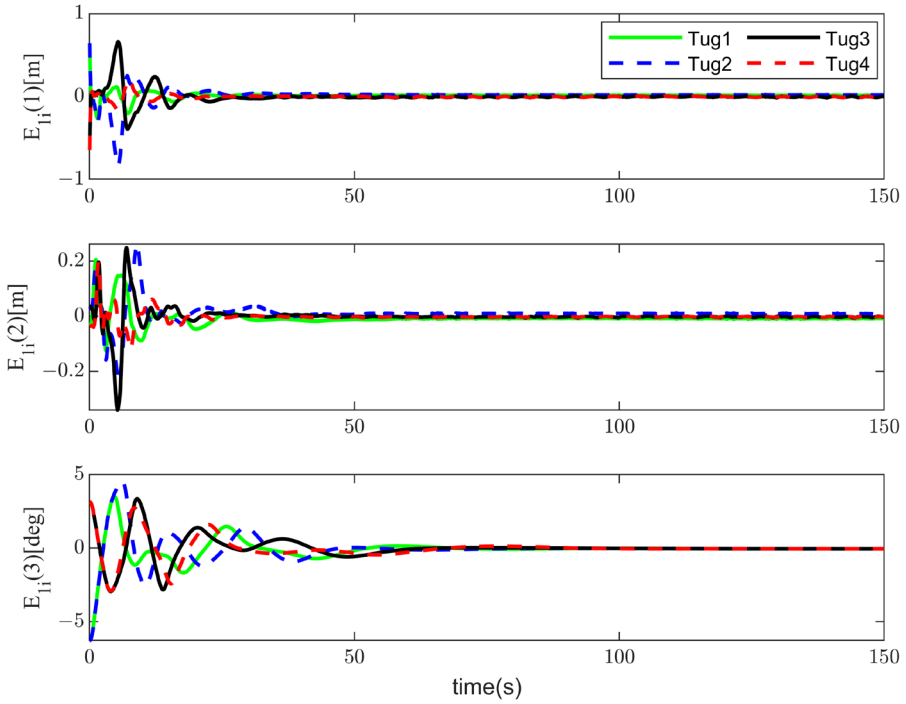

Figure 15. The position error curves of the tugs under CTC in **Case 1**.

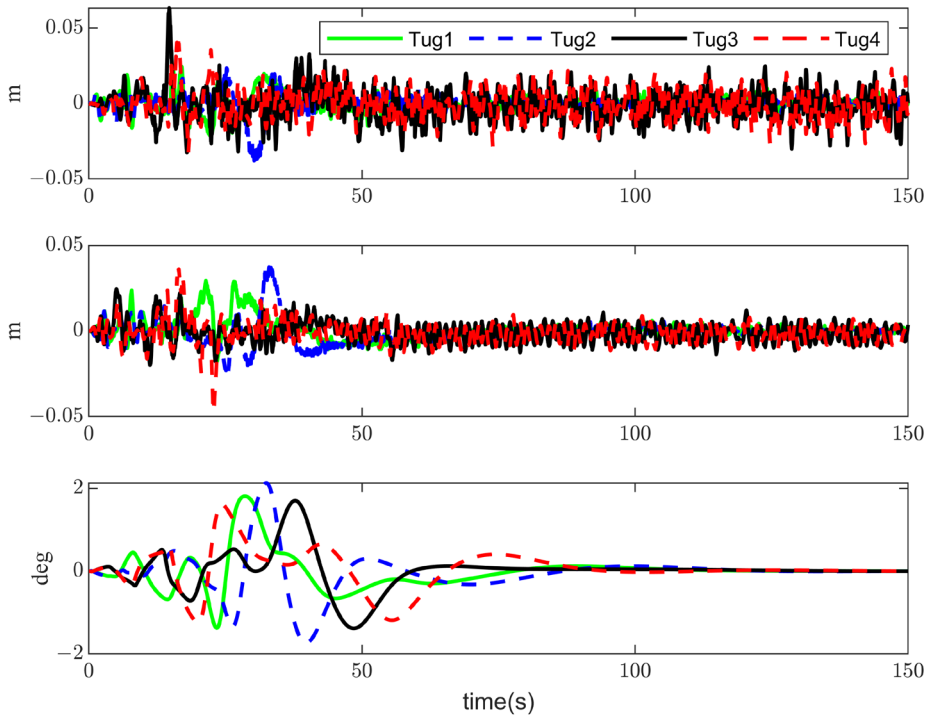

Figure 16. The deviation of tugs' position errors under two controllers (CTC and ETC) in Case 1.

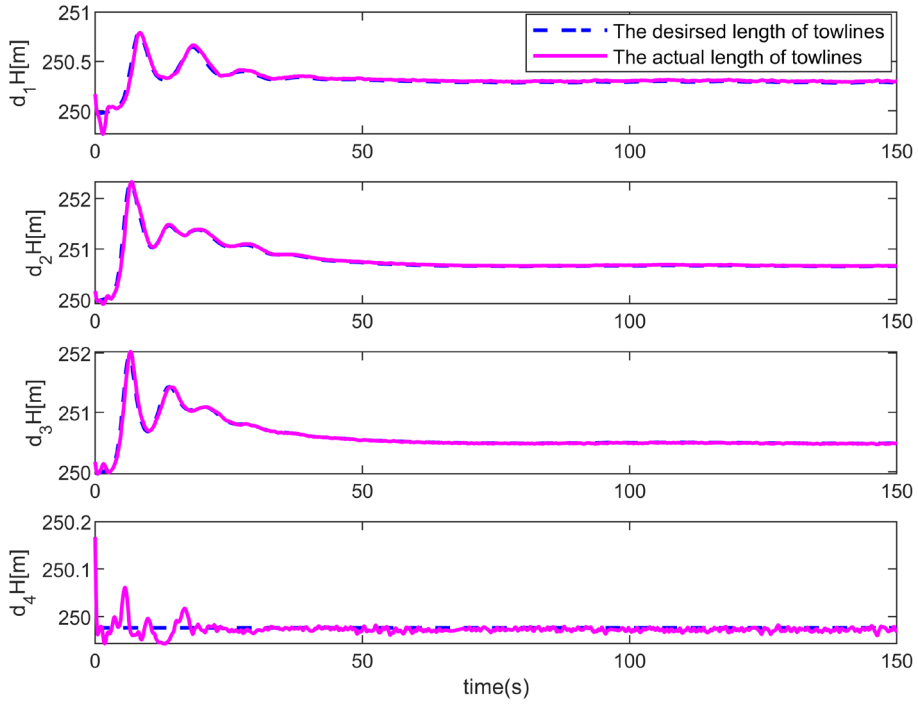

Figure 17. The horizontal lengths of four towlines under ETC in **Case 1**.

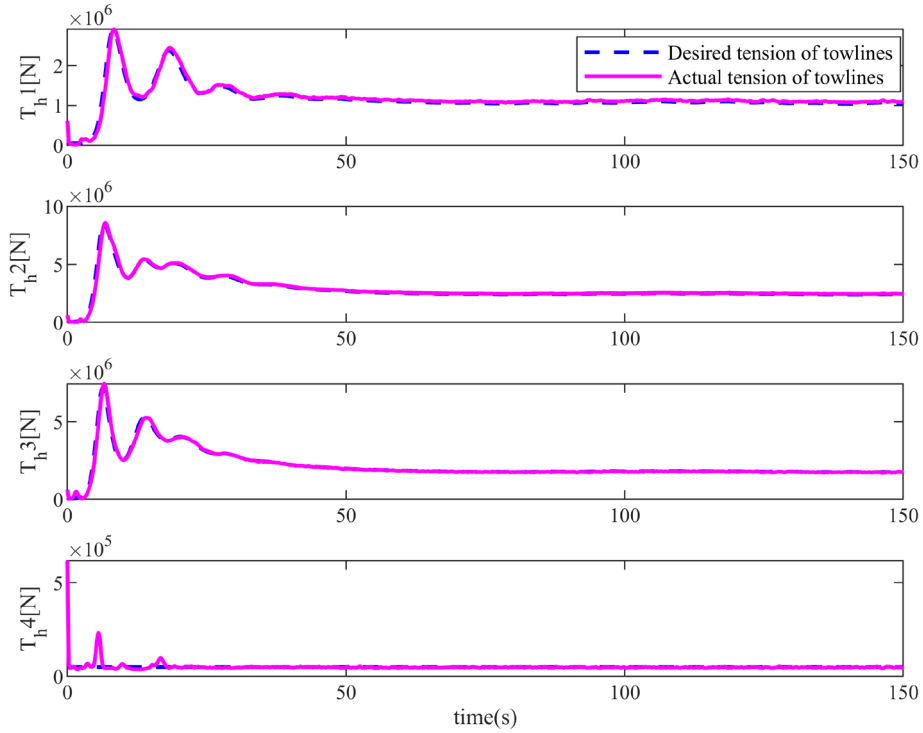

Figure 18. The horizontal tensions of four towlines under ETC in **Case 1**.

5. Conclusions

This paper proposed an event-triggered neural adaptive cooperative control for the TS with model parameter uncertainties and unknown disturbances. To begin with, we designed an adaptive RBFNN improved by the MLP algorithm to compensate for these uncertainties and disturbances. The MLP algorithm reduces the online learning parameters of the adaptive RBFNN to only three, significantly reducing the design and computation burden. Based on this adaptive RBFNN, we developed an event-triggered neural

adaptive virtual controller to obtain the desired drag force for the platform. Subsequently, according to the QP algorithm, the desired drag force is allocated as the desired tensions of the towlines. The desired towline lengths and the desired position information of the tugs are then obtained sequentially through the towline model and the position relationship between the tugs and the platform. Subsequently, an event-triggered neural adaptive distributed cooperative controller is designed for the tugs based on their desired positions. Simulations and analyses demonstrated that the event-triggered neural adaptive controllers can ensure the tracking error of the TS converges to a smaller neighborhood. The designed adaptive RBFNN with MLP requires only three online learning parameters, reducing the design and computational burden caused by numerous learning parameters and effectively compensating for uncertainties and disturbances in the TS. Additionally, the ETC mechanism reduces the communication burden within the TS and the execution frequency of the tugs' thrusters. In future research, we aim to design controllers with faster convergence rates under control input constraints and hope to conduct physical testing soon to further validate our proposed approaches.

Author Contributions: Methodology, S.G.; Formal analysis, Y.T.; Investigation, Y.T.; Writing – original draft, S.G. and Y.T.; Writing – review & editing, Y.T., Y.W. and S.W.; Supervision, Z.P. and S.W.; Funding acquisition, Y.T., Y.W., Z.P. and S.W.. All authors have read and agreed to the published version of the manuscript.

Funding: This study was supported in part by the National Key Research and Development Program of China (2022ZD0119902), in part by the National Natural Science Foundation of China (52101298, 52201409, 62273068, 51979020, 52271302), in part by the Dalian Innovative Support Scheme for High-level Talents (2023RQ066), in part by the Fundamental Research Funds for the Central Universities (3132023508), in part by the Key Basic Research of Dalian (2023JJ11CG008), and in part by the Natural Science Foundation of Liaoning Province (2023-MS-120).

Institutional Review Board Statement: Not applicable.

Informed Consent Statement: Not applicable.

Data Availability Statement: Data are contained within the article.

Acknowledgments: Our thanks to the hard-working editors, and for valuable comments from the reviewers.

Conflicts of Interest: The authors declare no conflict of interest.

Abbreviation

Key abbreviations and symbols used in this paper.

TS	Towing System
RBFNN	Radial basis function neural network
MLP	Minimal learning parameter
CTC	Continuous trigger control
ETC	Event-triggered control
QP	Quadratic programming
SHLNN	Single-hidden-layer neural network
$h(\delta)$	The neuron basis function
T_H	The horizontal tension
D_H	The horizontal length of the towlines
η_i , η_0	The positions of the tugs and platform
v_i , v_0	The velocity of the tugs and platform
$J(\psi_i)$, $J(\psi_0)$	The transformation matrices of the tugs and platform

M_i, M_0, D_i, D_i	The inertial and damping matrices of the tugs and platform
τ_w^i, τ_w^0, g_i, g_0	The disturbance forces and unmodeled dynamics of the tugs and platform
τ_h^i	The effort vector induced by the horizontal tension
η_i^{t-v}	The time-variant relative position
E_{1i}, E_{2i}, E_{10}, E_{20}	Position tracking errors and velocity tracking errors of the tugs and platform
ϑ_i, ϑ_0	The virtual controller of the tugs and platform
$\bar{\vartheta}_i$, $\bar{\vartheta}_0$	The output of first-order filter
$\boldsymbol{d}_i$, $\boldsymbol{d}_0$	The total disturbances and uncertainties of the tugs and platform
$\hat{\boldsymbol{d}}_i$, $\hat{\boldsymbol{d}}_0$	The estimation of RBFNN

References

1. Vu, M.T.; Choi, H.-S.; Kang, J.; Ji, D.-H.; Jeong, S.-K. A study on hovering motion of the underwater vehicle with umbilical cable. *Ocean Eng.* **2017**, *135*, 137–157.
2. Vu, M.T.; Le Thanh, H.N.N.; Huynh, T.T.; Thang, Q.; Duc, T.; Hoang, Q.D.; Le, T.H. Station-Keeping Control of a Hovering Over-Actuated Autonomous Underwater Vehicle under Ocean Current Effects and Model Uncertainties in Horizontal Plane. *IEEE Access* **2021**, *9*, 6855–6867.
3. Yu, Y.; Guo, C.; Yu, H. Finite-Time PLOS-Based Integral Sliding-Mode Adaptive Neural Path Following for Unmanned Surface Vessels with Unknown Dynamics and Disturbances. *IEEE Trans. Autom. Sci. Eng.* **2019**, *16*, 1500–1511.
4. Xia, G.; Sun, C.; Zhao, B. Output Feedback Cooperative Dynamic Positioning Control for an Unactuated Floating Object Using Multiple Vessels. *J. Mar. Sci. Eng.* **2021**, *9*, 463.
5. Du, Z.; Negenborn, R.R.; Reppa, V. Dynamic coordination of multiple vessels for offshore platform transportation. In Proceedings of the IEEE Conference on Control Technology and Applications, Trieste, Italy, 23–25 August 2022; pp. 76–81.
6. Bidikli, B.; Tatlicioglu, E.; Zergeroglu, E. Robust dynamic positioning of surface vessels via multiple unidirectional tugboats. *Ocean Eng.* **2016**, *113*, 237–245.
7. Braganza, D.; Feemster, M.; Dawson, D. Positioning of large surface vessels using multiple tugboats. In Proceedings of the American Control Conference, New York, NY, USA, 9–13 July 2007; pp. 912–917.
8. Esposito, J.M. Decentralized cooperative manipulation with a swarm of mobile robots. In Proceedings of the IEEE/RSJ International Conference on Intelligent Robots and Systems, St. Louis, MO, USA, 10–15 October 2009; pp. 5333–5338.
9. Choi, J.K. Path-following control of a ship by pushing using a single autonomous tugboat. *J. Mar. Sci. Technol.* **2023**, *28*, 64957.
10. Xia, G.; Sun, C.; Zhao, B.; Sun, X.; Xia, X. Robust cooperative trajectory tracking control for an unactuated floating object with multiple vessels system. *ISA Trans.* **2022**, *123*, 263–271.
11. Sun, M.; Luan, T.; Liang, L. RBF neural network compensation-based adaptive control for lift-feedback system of ship fin stabilizers to improve anti-rolling effect. *Ocean Eng.* **2018**, *163*, 307–321.
12. Shu, R.; Jia, Q.; Wu, Y.; Liao, H.; Zhang, C. Robust Active Fault-Tolerant Configuration Control for Spacecraft Formation via Learning RBFNN Approaches. *J. Aerosp. Eng.* **2024**, *37*, 04024007.
13. Jin, X.-Z.; Lu, S.-Y.; Che, W.-W.; Deng, C.; Chi, J. Robust adaptive radial-basis function neural network-based backstepping control of a class of perturbed nonlinear systems with unknown system parameters. *Int. J. Robust Nonlinear Control* **2021**, *31*, 5101–5117.
14. Dai, S.-L.; He, S.; Ma, Y.; Yuan, C. Distributed cooperative learning control of uncertain multiagent systems with prescribed performance and preserved connectivity. *IEEE Trans. Neural Netw. Learn. Syst.* **2021**, *32*, 3217–3229.
15. Zou, A.-M.; Kumar, K.D.; Hou, Z.-G.; Liu, X. Finite-Time Attitude Tracking Control for Spacecraft Using Terminal Sliding Mode and Chebyshev Neural Network. *IEEE Trans. Syst. Man Cybern. Part B (Cybern.)* **2011**, *41*, 950–963.
16. Van, M. Adaptive neural integral sliding-mode control for tracking control of fully actuated uncertain surface vessels. *Int. J. Robust Nonlinear Control* **2019**, *29*, 1537–1557.
17. Poursadegh, A.; Shahnazi, R. Optimal Neuro-adaptive Funnel Heading Control for Marine Vessels Subject to Dead-zone Actuator. In Proceedings of the 2020 28th Iranian Conference on Electrical Engineering (ICEE), Tabriz, Iran, 4–6 August 2020; pp. 1–6.
18. Tuo, Y.; Wang, S.; Guo, C.; Yu, H.; Shen, Z. Reliability-based event driven backstepping positioning control for a turret-moored FPSO vessel with unknown slow time-varying disturbances. *Int. J. Control Autom. Syst.* **2022**, *20*, 472–482.
19. Aspragkathos, S.N.; Karras, G.C.; Kyriakopoulos, K.J. Ensuring Safety for UAVs Through Event-Triggered Predictive Control. In Proceedings of the 2024 32nd Mediterranean Conference on Control and Automation (MED), Chania, Greece, 11–14 June 2024; pp. 185–190.

20. Wang, J.; Xu, Y.; Xu, Y.; Yang, D. Time-varying formation for high-order multi-agent systems with external disturbances by event-triggered integral sliding mode control. *Appl. Math. Comput.* **2019**, *359*, 333–343.
21. Zhou, B.; Huang, B.; Su, Y.; Zhu, C. Interleaved periodic event-triggered communications-based distributed formation control for cooperative unmanned surface vessels. *IEEE Trans. Neural Netw. Learn. Syst.* **2024**, 1–13. 10.1109/TNNLS.2024.3351218
22. Williams, D.A.; Chapman, A.; Manzie, C. Generalized Asynchronous Event-Triggered Measurement and Control for Non-Linear Systems. In Proceedings of the 2024 Australian & New Zealand Control Conference (ANZCC), Gold Coast, Australia, 1–2 February 2024; pp. 1–6.
23. Seshagiri, S.; Khalil, H.K. Output feedback control of nonlinear systems using RBF neural networks. *IEEE Trans. Neural Netw.* **1999**, *4*, 2808–2812.
24. Tao, J.; Du, L.; Dehmer, M.; Wen, Y.; Xie, G.; Zhou, Q. Path following control for towing system of cylindrical drilling platform in presence of disturbances and uncertainties. *ISA Trans.* **2019**, *95*, 185–193.
25. Chen, L.; Hopman, H.; Negenborn, R.R. Distributed model predictive control for cooperative floating object transport with multi-vessel systems. *Ocean Eng.* **2019**, *191*, 106515.
26. Fossen, T.I. *Marine Control Systems: Guidance, Navigation, and Control of Ships, Rigs and Underwater Vehicles*; Marine Cybernetics, Trondheim, Norway; Springer: Berlin/Heidelberg, Germany, 2002.
27. Postoyan, R.; Bragagnolo, M.C.; Galbrun, E. Event-triggered tracking control of unicycle mobile robots. *Automatica* **2015**, *52*, 302–308.
28. Girada, A. Dynamic triggering mechanisms for event triggered control. *IEEE Trans. Autom. Control* **2015**, *60*, 1992–1997.
29. Bekhit, N.M.; Emam, O.E.; Elhamid, L.A. A Multi-Level Multi-Objective Integer Quadratic Programming Problem Under Pentagonal Neutrosophic Environment. *Fuzzy Inf. Eng.* **2023**, *15*, 347–361.
30. Arnström, D.; Bemporad, A.; Axehill, D. A Linear Programming Method Based on Proximal-Point Iterations with Applications to Multi-Parametric Programming. *IEEE Control Syst. Lett.* **2022**, *6*, 2066–2071.
31. Dalman, H.; Bayram, M. Interactive Fuzzy Goal Programming Based on Taylor Series to Solve Multiobjective Nonlinear Programming Problems with Interval Type-2 Fuzzy Numbers. *IEEE Trans. Fuzzy Syst.* **2018**, *26*, 2434–2449.
32. Fang, X.; Xie, L. Distributed Formation Maneuver Control Using Complex Laplacian. *IEEE Trans. Autom. Control* **2024**, *69*, 1850–1857.
33. Xia, G.; Sun, C.; Zhao, B.; Xue, J. Cooperative control of multiple dynamic positioning vessels with input saturation based on finite time disturbance observer. *Int. J. Control Autom. Syst.* **2019**, *17*, 370–379.
34. Fu, M.; Yu, L. Finite-time extended state observer-based distributed formation control for marine surface vehicles with input saturation and disturbances. *Ocean Eng.* **2018**, *159*, 219–227.
35. Fossen, T.I.; Strand, J.P. Passive nonlinear observer design for ships using Lyapunov methods: Full-scale experiments with a supply vessel. *Automatica* **1999**, *35*, 3–16.